Article

Spectroscopic and Computational Studies of Ni Superoxide Dismutase: Electronic Structure Contributions to Enzymatic Function

Adam T. Fiedler, Peter A. Bryngelson, Michael J. Maroney, and Thomas C. Brunold

J. Am. Chem. Soc., **2005**, 127 (15), 5449-5462• DOI: 10.1021/ja042521i • Publication Date (Web): 25 March 2005

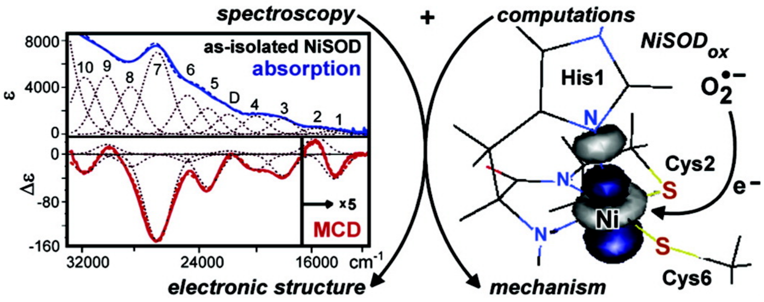

Journal of the American Chemical Society is published by the American Chemical Society. 1155 Sixteenth Street N.W., Washington, DC 20036

J|A|C|S
ARTICLES
Published on Web 03/25/2005

Spectroscopic and Computational Studies of Ni Superoxide Dismutase: Electronic Structure Contributions to Enzymatic Function

Adam T. Fiedler,[†] Peter A. Bryngelson,[‡] Michael J. Maroney,[‡] and Thomas C. Brunold*,[†]

Contribution from the University of Wisconsin-Madison, Department of Chemistry, Madison, Wisconsin 53706, and University of Massachusetts, Department of Chemistry, Amherst, Massachusetts 01003

Received December 13, 2004; E-mail: brunold@chem.wisc.edu

Abstract: Ni-containing superoxide dismutase (NiSOD) is the most recently discovered member of the class of metalloenzymes that detoxify the superoxide radical in aerobic organisms. In this study, we have employed a variety of spectroscopic and computational methods to probe the electronic structure of the NiSOD active site in both its oxidized (NiSOD$_{ox}$, possessing a low-spin ($S = {}^1/_2$) Ni^{3+} center) and reduced (NiSOD$_{red}$, containing a diamagnetic Ni^{2+} center) states. Our experimentally validated computed electronic-structure description for NiSOD$_{ox}$ reveals strong σ-bonding interactions between Ni and the equatorial S/N ligands, which give rise to intense charge-transfer transitions in the near-UV region of the absorption spectrum. Resonance Raman (rR) spectra obtained with laser excitation in this region exhibit two features at 349 and 365 cm^{-1} that are assigned to Ni$-$S$_{Cys}$ stretching modes. The NiSOD$_{red}$ active site also exhibits a high degree of metal$-$ligand bond covalency as well as filled/filled π-interactions between Ni and S/N orbitals, which serve to adjust the redox potential of the Ni^{2+} center. Comparison of our computational results for NiSOD$_{red}$ with those obtained in parallel studies of synthetic [NiS$_2$N$_2$] complexes reveals that the presence of an anionic N-donor ligand is crucial for promoting metal-based (versus S-based) oxidation of the active site. The implications of our electronic-structure descriptions with respect to the function of NiSOD are discussed, and a comparison of M$-$S$_{Cys}$ bonding in NiSOD and other metalloenzymes with sulfur ligation is provided.

Introduction

The anionic superoxide radical (O$_2$$^{\bullet-}$) is an inevitable byproduct of aerobic metabolism that, if not eliminated, may cause significant cellular damage; consequently, superoxide has been implicated in numerous medical disorders.[1] To avoid such harmful consequences, all aerobic organisms possess metalloenzymes known as superoxide dismutases (SODs) that disproportionate the toxic O$_2$$^{\bullet-}$ radical to molecular oxygen and hydrogen peroxide.[2] All SODs employ the two-step, ping-pong mechanism shown in eq 1, where M is a redox-active metal center capable of both oxidizing and reducing superoxide:

$$\mathbf{M^{ox}} + \mathrm{O_2}^{\bullet-} \rightarrow \mathbf{M^{red}} + \mathrm{O_2} \qquad (1a)$$

$$\mathbf{M^{red}} + \mathrm{O_2}^{\bullet-} + 2\mathrm{H}^+ \rightarrow \mathbf{M^{ox}} + \mathrm{H_2O_2} \qquad (1b)$$

While SODs possessing Fe, Mn, and Cu/Zn active sites have been studied extensively for years, the past decade has witnessed the emergence of an additional class of Ni-containing SODs (NiSODs), which are found in *Streptomyces* species[3,4] and cyanobacteria.[5] In most organisms, NiSODs function as a homohexamer composed of ~13 kDa subunits.[6,7] Initial studies of NiSOD with EPR spectroscopy revealed that the metal center cycles between diamagnetic Ni^{2+} and paramagnetic ($S = {}^1/_2$) Ni^{3+} states, and the observation of superhyperfine splittings suggested the presence of axial nitrogen coordination in the oxidized state.[3,8] Additional studies with X-ray absorption

---

[†] University of Wisconsin-Madison.

[‡] University of Massachusetts.

(1) (a) McCord, J. M. *Superoxide Dismutase* **2002**, *349*, 331−341. (b) Beyer, W.; Imlay, J.; Fridovich, I. *Prog. Nucleic Acid Res. Mol. Biol.* **1991**, *40*, 221−253. (c) Wallace, D. C. *Science* **1992**, *256*, 628−632. (d) Winterbourn, C. C. *Free Radical Biol. Med.* **1993**, *14*, 85−90. (e) Halliwell, B. In *Active Oxygen in Biochemistry*; Valentine, J. S., Foote, C. S., Greenberg, A., Liebman, J. F., Eds.; Blackie Academic and Professional: New York, 1995; pp 313−335.

(2) (a) Fridovich, I. *Annu. Rev. Biochem.* **1995**, *64*, 97−112. (b) Miller, A. F. *Comments Mol. Cell. Biophys.* **1997**, *9*, 1−48. (c) Valentine, J. S.; Wertz, D. L.; Lyons, T. J.; Liou, L.; Goto, J. J.; Gralla, E. B. *Curr. Opin. Chem. Biol.* **1998**, *2*, 253−262. (d) Miller, A. F. *Curr. Opin. Chem. Biol.* **2004**, *8*, 162−168.

(3) Youn, H. D.; Kim, E. J.; Roe, J. H.; Hah, Y. C.; Kang, S. O. *Biochem. J.* **1996**, *318*, 889−896.

(4) Youn, H. D.; Youn, H.; Lee, J. W.; Yim, Y. I.; Lee, J. K.; Hah, Y. C.; Kang, S. O. *Arch. Biochem. Biophys.* **1996**, *334*, 341−348.

(5) Palenik, B.; Brahamsha, B.; Larimer, F. W.; Land, M.; Hauser, L.; Chain, P.; Lamerdin, J.; Regala, W.; Allen, E. E.; McCarren, J.; Paulsen, I.; Dufresne, A.; Partensky, F.; Webb, E. A.; Waterbury, J. *Nature* **2003**, *424*, 1037−1042.

(6) Barondeau, D. P.; Kassmann, C. J.; Bruns, C. K.; Tainer, J. A.; Getzoff, E. D. *Biochemistry* **2004**, *43*, 8038−8047.

(7) Wuerges, J.; Lee, J. W.; Yim, Y. I.; Yim, H. S.; Kang, S. O.; Carugo, K. D. *Proc. Natl. Acad. Sci. U.S.A.* **2004**, *101*, 8569−8574.

(8) Choudhury, S. B.; Lee, J. W.; Davidson, G.; Yim, Y. I.; Bose, K.; Sharma, M. L.; Kang, S. O.; Cabelli, D. E.; Maroney, M. J. *Biochemistry* **1999**, *38*, 3744−3752.

10.1021/ja042521i CCC: $30.25 © 2005 American Chemical Society

Scheme 1. Structures of NiSOD Active Site in Oxidized (Top) and Reduced (Bottom) States

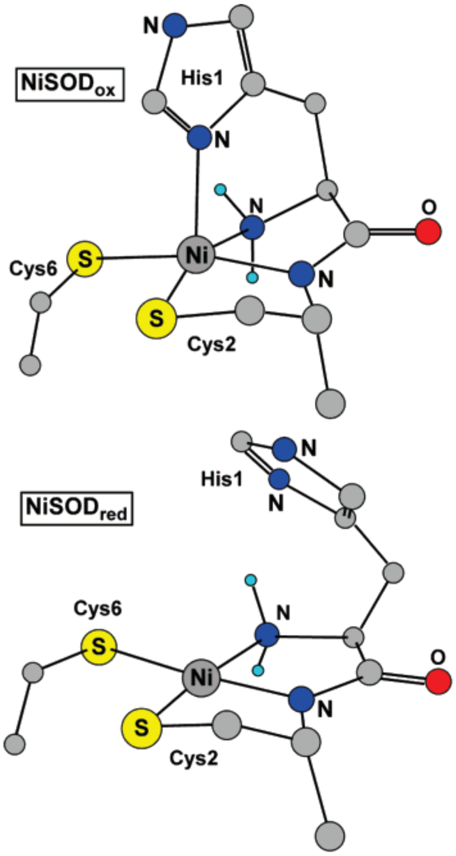

spectroscopy (XAS) revealed that the number of Ni ligands changes as a function of metal oxidation state and that the metal coordination environment is comprised of multiple S-donor ligands.[8] The latter discovery was quite unexpected, as sulfur-containing molecules are susceptible to modification and degradation by oxidants such as superoxide and its derivatives, and none of the previously characterized SODs contain sulfur ligation. While a binuclear Ni active site with mixed thioether/thiolate ligation was among the structures originally proposed,[8] further XAS studies led to the conclusion that this site is in fact mononuclear and possesses terminal Cys ligands.[9]

Two recent X-ray crystallographic studies of NiSODs from *Streptomyces* species have further elucidated the nature of the enzyme active site (Scheme 1).[6,7] In both structures, the square-pyramidal coordination geometry exhibited by the Ni center in the oxidized form (NiSOD$_{ox}$) is converted to a square-planar geometry in the reduced state (NiSOD$_{red}$), as the axial imidazole group derived from the His1 residue dissociates upon metal ion reduction. The four equatorial ligands include two thiolates from Cys2 and Cys6 in a cis arrangement, the deprotonated amide of the Cys2 backbone, and the N-terminal $-NH_2$ group of His1. The involvement of this last ligand necessitates the post-translational removal of 14 N-terminal amino acids to yield a protein capable of binding Ni.[6,10] In the oxidized state, the bond distance between Ni and the N_δ atom of His1 is quite lengthy, ranging from 2.3 to 2.6 Å in the two structures. It appears that this axial imidazole group experiences hydrogen-bonding interactions with several second-sphere residues and may be protonated (positively charged) in the reduced state.[6,7]

While remarkable progress has been made toward elucidating the structure of NiSOD, fundamental questions remain regarding the functional properties of this enzyme. First, the nature of the enzymatic mechanism, inner-sphere versus outer-sphere, is still a matter of dispute. Based on the positions of three conserved Lys residues, Getzoff and co-workers have argued for the existence of an active-site channel that electrostatically steers the substrate toward the Ni center,[6] consistent with an inner-sphere mechanism. In contrast, no evidence for electrostatic guidance was found by Wuerges et al.[7], a result corroborated by previous studies that demonstrated a lack of dependence of k_{cat} on ionic strength.[8] Furthermore, the active site was deemed to be inaccessible to solvent, suggesting an outer-sphere mechanism.[7] Another mechanistic issue pertains to the source of the protons required in the substrate reduction step of the SOD mechanism (eq 1b). While second-sphere residues such as Tyr9 are attractive candidates to serve this role,[6] others have suggested that the first-sphere thiolate[8,9] and imidazole[10] ligands could also function in proton transfer to the nascent peroxide.

When compared to other members of the SOD family, NiSOD exhibits numerous structural features that are unique and warrant further investigation. As noted above, thiolate ligation is unique to NiSODs, and it remains unclear how the enzyme prevents sulfur-based oxidation, especially if an inner-sphere mechanism is at work. NiSOD is also the only SOD (with the possible exception of the Cu/Zn enzyme[11]) to exhibit changes in metal coordination number that are oxidation-state dependent, and the labile imidazole group of His1 clearly plays a crucial role in the enzymatic mechanism, as mutations of this residue greatly depress catalytic activity.[10] Yet interesting commonalities also exist across the various SODs. For instance, in analogy with Fe- and MnSODs,[12] hydrogen-bonding interactions between first- and second-sphere residues in the Ni enzyme appear to be crucial for maximizing catalytic turnover.[6,7]

While the three-dimensional structure of the NiSOD active site is now well-established, many of the unresolved issues described above can only be addressed through detailed exploration of the corresponding electronic properties. Herein, we report combined spectroscopic/computational investigations of the oxidized and reduced NiSOD enzyme. Specifically, electronic absorption, circular dichroism (CD), magnetic circular dichroism (MCD), and resonance Raman (rR) spectroscopies have been used to establish an experimental framework for evaluating density functional theory (DFT) and semiempirical INDO/S-CI calculations. This is the first examination of NiSOD with optical and vibrational spectroscopies, as well as the first application of computational methods to this system. This combination of spectroscopic and computational techniques allowed us to generate experimentally validated electronic-structure descriptions of the NiSOD active site in both the oxidized and reduced states. To further our understanding of key bonding interactions,

---

(9) Szilagyi, R. K.; Bryngelson, P. A.; Maroney, M. J.; Hedman, B.; Hodgson, K. O.; Solomon, E. I. *J. Am. Chem. Soc.* **2004**, *126*, 3018−3019.

(10) Bryngelson, P. A.; Arobo, S. E.; Pinkham, J. L.; Cabelli, D. E.; Maroney, M. J. *J. Am. Chem. Soc.* **2004**, *126*, 460−461.

(11) Hart, P. J.; Balbirnie, M. M.; Ogihara, N. L.; Nersissian, A. M.; Weiss, M. S.; Valentine, J. S.; Eisenberg, D. *Biochemistry* **1999**, *38*, 2167−2178.

(12) (a) Yikilmaz, E.; Xie, J.; Brunold, T. C.; Miller, A. F. *J. Am. Chem. Soc.* **2002**, *124*, 3482−3483. (b) Vance, C. K.; Miller, A. F. *Biochemistry* **2001**, *40*, 13079−13087. (c) Vance, C. K.; Miller, A. F. *J. Am. Chem. Soc.* **1998**, *120*, 461−467.

our approach was also applied to well-characterized, synthetic Ni complexes with N/S ligation that offer excellent reference systems for comparison with the protein active site. Collectively, these studies provide significant insight into the mechanisms by which the axial and equatorial ligands tune the reactivity of the Ni center for optimum catalytic activity. Starting from our experimentally calibrated active-site models of the resting states, our computational tools were also used to assess the ability of the thiolate ligands to bind protons and to probe the effect of second-sphere residues on the electronic structure of the active site. The implications of the insights gained in these studies for the function and mechanism of NiSOD are discussed, and the spectral and electronic properties of this enzyme are compared with those reported for other metalloproteins possessing metal−thiolate ligation, including the blue copper and superoxide reductase proteins.

Experimental and Computational Methods

Expression, Purification, and Reconstitution of NiSOD. Recombinant NiSOD was expressed as an N-terminal fusion peptide in a manner similar to that previously described.[10] Cultures of *E. coli* expressing the fusion protein (H15) of WT NiSOD were grown to an OD of 0.6 at 550 nm and induced (0.8 mM isopropyl-β-D-thiogalactopyranoside) for 3 h. Cells were harvested by centrifugation, resuspended in 50 mL of Ni-NTA bind buffer (10 mM imidazole, 50 mM sodium phosphate, 300 mM sodium chloride pH 8.0) with 1 mM phenylmethylsulfonyl fluoride (PMSF), and frozen at −80 °C. Aliquots of cells were thawed, and 100 μL of DNAse I solution (10 mg/mL DNAse I, 10 mM magnesium chloride, 20 mM Tris pH 7.5, 40% glycerol) were added and incubated at 37 °C for 25 min or until the viscosity of the solution was significantly reduced. All chromatographic purifications employed an Amersham Biosciences FPLC with UV detector. The cell lysate was centrifuged, and the supernatant was then loaded onto a column (Pharmacia HR10) containing Ni−NTA His•Bind Superflow resin (Novagen) at 1.5 mL/min with bind buffer. The loading was monitored at 280 nm, and when the signal returned to the baseline, a step gradient was applied of 30% elute buffer (250 mM imidazole, 50 mM sodium phosphate, 300 mM sodium chloride, pH 8.0) and the column was washed with 7 volumes of buffer. Following the wash step, the fusion protein was eluted from the column with 100% elute buffer. The eluted protein was then dialyzed against 20 mM Tris buffer pH 8.5. Subsequently the fusion protein was dialyzed exhaustively against factor Xa cleavage buffer (5 mM calcium chloride, 50 mM Tris, 100 mM sodium chloride, pH 8.0) containing 0.2 mM PMSF.

Following purification, the N-terminal fusion peptide was removed. Fusion protein in factor Xa cleavage buffer was divided into 1 mL aliquots. Factor Xa was added to the buffer at a concentration of 1 unit/50 μg of fusion protein. The cleavage reaction was left at 4 °C for 4 days. Cleavage was monitored by SDS-PAGE.

Reconstitution of the N-terminal processed recombinant apo-NiSOD was achieved under anaerobic conditions (Coy chamber). The protein was first reduced by addition of a 5-fold excess of dithiothreitol. The reduction was allowed to proceed for 2−3 h. Subsequent addition of a 3-fold excess of $NiCl_2$ resulted in the formation of hexameric active enzyme. Anion exchange chromatography (FPLC, using a Mono Q column) using Tris buffer at pH 8.5 with a 0.5 M sodium chloride gradient over 20 column volumes and a flow rate of 0.5 mL/min gave homogeneous (SDS-PAGE) holo-NiSOD in the first fractions off the column.

Spectroscopy. Room-temperature absorption spectra were collected with a Varian Cary 5E UV−vis−NIR spectrophotometer. Variable-temperature absorption, CD, and MCD spectra were recorded using a Jasco J-715 spectropolarimeter in conjunction with an Oxford Instruments SM-4000 8T magnetocryostat. All MCD spectra reported herein were obtained by subtracting the −7 T spectrum from the +7 T spectrum to eliminate CD contributions. Protein samples used for low-temperature absorption and MCD studies were prepared in ~50% (v/v) mixtures of glycerol and the appropriate buffer. The azide-treated sample was formed by addition of 10 μL of an aqueous NaN_3 solution (3 M) to 100 μL of as-isolated NiSOD (1.4 mM), yielding a solution with a N_3^-/Ni ratio of ~200:1. Samples of reduced NiSOD were prepared by treating 100 μL of as-isolated NiSOD (1.4 mM) with 10 μL of an aqueous dithionite solution (200 mM).

Resonance Raman (rR) spectra were obtained upon excitation with a Coherent I-302C Kr^+ laser with ~30−60 mW of laser power at the sample. The scattered light was collected using a ~135° backscattering arrangement, dispersed by an Acton Research triple monochromator equipped with a 2400 groves/mm grating and analyzed with a Princeton Instruments Spec X: 100BR deep depletion, back-thinned CCD camera. Spectra at 77 and 273 K were obtained by placing the sample-containing NMR tube in an EPR dewar filled with liquid N_2 and ice, respectively, to prevent sample degradation during data collection. Sample concentration was ~1−2 mM.

Computations. Active-site models of NiSOD were generated by constrained DFT geometry optimizations using the Amsterdam Density Functional (ADF) 2002.03 software package.[13] Initial structures for these optimizations were derived from published X-ray crystallographic data of NiSOD.[6,7] As shown in Figure 5, in all models the Cys6 residue was modeled as ethyl thiolate ($\mathbf{C}H_3CH_2S^-$), and the C═O unit of Cys2 was replaced with either a —H or —$\mathbf{C}H_3$ moiety. In structures that incorporated second-sphere residues, Glu17 and Arg47 were modeled as $\mathbf{C}H_3$—CO_2^- and $\mathbf{C}H_3$—$\mathbf{N}$H—$C(NH_2)_2^+$, respectively. The atoms in **bold** were fixed to their crystallographically determined positions and not allowed to move in the course of the geometry optimizations. DFT structural refinements of the synthetic complexes used the corresponding X-ray crystal structures as their starting points, and the positions of all atoms were allowed to vary. The resulting geometries agree well with the crystallographic data obtained for the Ni^{2+} complexes, although DFT slightly overestimates Ni-ligand bond distances (Table S4). All optimizations were carried out on a cluster of 20 Intel Xeon processors (Ace computers) using ADF basis set IV (triple-ζ with single polarization), an integration constant of 4.0, and the Vosko−Wilk−Nusair local density approximation[14] with the nonlocal gradient corrections of Becke[15] and Perdew.[16] The Cartesian coordinates for all DFT geometry-optimized models of oxidized and reduced NiSOD mentioned in the text are available in the Supporting Information (Tables S2a−h), along with those obtained for the synthetic Ni complexes **1**−**3** (Tables S3a−e).

All single-point DFT calculations were performed using the ORCA 2.2 software package developed by Dr. F. Neese.[17] Computations on paramagnetic (formally) Ni^{3+}-containing species were carried out using the spin-unrestricted formalism, while those on diamagnetic, Ni^{2+}-containing species were performed spin-restricted. The computations utilized Ahlrichs' valence triple-ζ basis set[18] with one set of polarization functions[19] (TZV/P) on all atoms, in conjunction with the corresponding auxiliary basis set (TZV/C),[20] and employed Becke's three-parameter hybrid functional[21] for exchange along with the Lee−Yang−Parr

---

[13] (a) Baerends, E. J.; Ellis, D. E.; Ros, P. *Chem. Phys.* **1973**, *2*, 41. (b) Guerra, C. F.; Snijders, J. G.; te Velde, G.; Baerends, E. J. *Theor. Chem. Acc.* **1998**, *99*, 391−403. (c) te Velde, G.; Baerends, E. J. *J. Comput. Phys.* **1992**, *99*, 84−98. (d) Versluis, L.; Ziegler, T. *J. Chem. Phys.* **1988**, *88*, 322−328.

[14] Vosko, S. H.; Wilk, L.; Nusair, M. *Can. J. Phys.* **1980**, *58*, 1200−1211.

[15] Becke, A. D. *J. Chem. Phys.* **1986**, *84*, 4524−4529.

[16] Perdew, J. P. *Phys. Rev. B: Condens. Matter* **1986**, *33*, 8822−8824.

[17] Neese, F. *ORCA*, version 2.2.; an ab initio, density functional, and semiempirical program package; Max-Plack Institut für Bioanorganische Chemie: Mülheim an der Ruhr, Germany, 2001.

[18] Schaefer, A.; Horn, H.; Ahlrichs, R. *J. Chem. Phys.* **1992**, *97*, 2571.

[19] Ahlrichs, R. Unpublished results.

[20] (a) Eichkorn, K.; Treutler, O.; Ohm, H.; Haser, M.; Ahlrichs, R. *Chem. Phys. Lett.* **1995**, *240*, 283. (b) Eichkorn, K.; Weigend, F.; Treutler, O.; Ahlrichs, R. *Theor. Chem. Acc.* **1997**, *97*, 119.

correlation functional[22] (B3LYP) with an integration grid of 4.0. The gOpenMol program[23] developed by Laaksonen was used to generate isosurface plots of molecular orbitals (using an isodensity value of 0.05 $(e/b^3)^{1/2}$). To facilitate comparison of orbital energies, single-point calculations of the **ox^2** and **ox^3** models used the structures derived from the corresponding ADF optimizations but omitted the atoms of second-sphere residues.

EPR parameters for the NiSOD$_{ox}$ models and the synthetic complex **3** were computed with the ORCA program by solving the coupled-perturbed SCF (CP-SCF) equations[24] and using the B3LYP hybrid functional described above. For these calculations, three types of basis sets were used: (i) Kutzelnigg's NMR/EPR (IGLO-III) basis set[25] for all ligating N atoms, (ii) Ahlrichs' valence triple-ζ basis set[18] with two sets of polarization functions[19] (TZV/PP) for the Ni and S atoms, and (iii) Ahlrichs' valence triple-ζ basis set[18] with one set of polarization functions[19] (TZV/P) for all remaining atoms. The CP-SCF calculations of the **g**-matrix included all orbitals within a ±100 hartree window of the HOMO/LUMO energy gap, with the origin of the matrix defined by the center of electronic charge. A high-resolution radial grid with an integration accuracy of 7.0 was used for Ni and all N atoms.

Semiempirical calculations employing the INDO/S model developed by Zerner and co-workers[26] were also performed using the ORCA program. The calculations used the valence-shell ionization potentials and Slater−Condon parameters listed by Bacon and Zerner[27] and the standard interaction factors $f_{p\sigma p\sigma} = 1.266$ and $f_{p\pi p\pi} = 0.585$. Restricted open-shell Hartree−Fock (ROHF) SCF calculations were converged on the spin doublet ground states of the Ni^{3+} models, which served as the reference states for configuration interaction (CI) calculations. Calculations of electronic transition energies and intensities included single-electron excitations from all doubly occupied MOs (DOMOs) within 5 eV of the HOMO to the singly occupied MO (SOMO) and virtual MOs within 5 eV of the LUMO.

Results and Analysis

Spectroscopic Results. The low-temperature (15 K) electronic absorption spectrum of as-isolated NiSOD (Figure 1, top) is dominated by an intense band in the near-UV region ($\nu_{max} = 26\,900$ cm^{-1}). To lower energy, three shoulders are observed at ~24 200, 19 700, and 15 500 cm^{-1} that become progressively weaker with decreasing energy. Based upon EPR spin-quantization experiments[3,8] and recent crystallographic results,[6] as-isolated samples of NiSOD contain approximately equal amounts of Ni^{2+}- and Ni^{3+}-bound active sites, and thus both oxidation states contribute to the corresponding absorption spectrum. To approach this problem, contributions from the oxidized component to the as-isolated spectrum were resolved by subtracting the absorption spectrum of reduced NiSOD, which was obtained by treatment of the as-isolated protein with dithionite (DTH) (Figure 2, top). Because the reduced enzyme exhibits relatively weak absorption intensity (ϵ < 1500 M^{-1} cm^{-1}) over the relevant energy range, the overall shape of the NiSOD$_{ox}$ absorption spectrum is virtually identical to that of the as-isolated protein (see Figure S1). Specifically, the intense peak at 26 900 cm^{-1} ($\epsilon \approx 8000$ M^{-1} cm^{-1}) and the majority of the lower-energy features arise entirely from the oxidized enzyme.

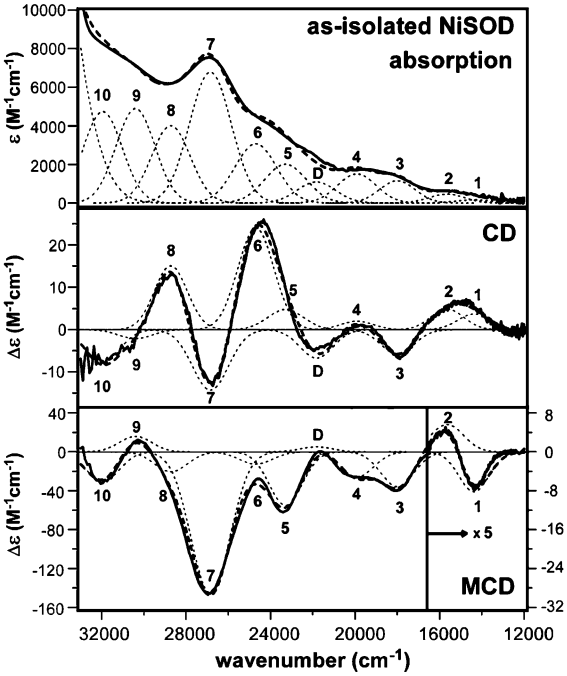

Figure 1. Solid lines: electronic absorption (top), CD (middle), and 7 T MCD (bottom) spectra of as-isolated NiSOD. Dotted lines: Gaussian deconvolutions of the experimental spectra, with the overall fit shown with the dashed lines. The absorption spectrum was collected at a temperature of 15 K, while the remaining spectra were obtained at 4 K. Band energies and parameters are summarized in Table 1. The ϵ_{abs} and $\Delta\epsilon$ values provided pertain to NiSOD$_{ox}$ and were obtained under the assumption that as-isolated NiSOD is an equal mixture of oxidized and reduced protein (see captions of Figures S1 and S2 for more details).

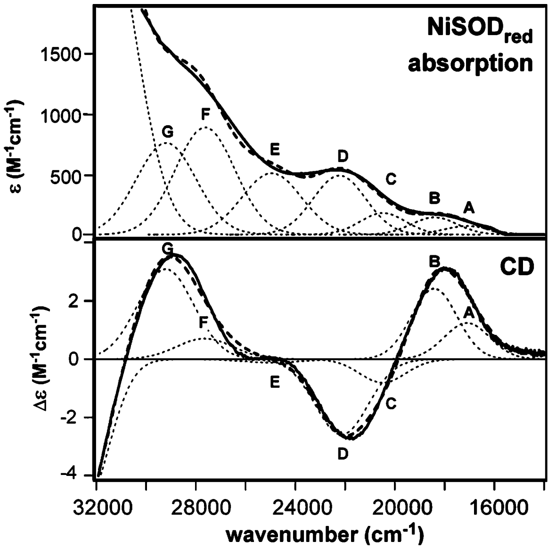

Figure 2. Solid lines: electronic absorption (top) and CD (bottom) spectra of dithionite-reduced NiSOD. Dotted lines: Gaussian deconvolutions of the experimental spectra, with the overall fit shown with the dashed lines. All spectra were obtained at room temperature. Band energies and parameters are summarized in Table 1.

The corresponding CD and MCD spectra (Figure 1) allow for resolution of the numerous bands that comprise the absorption spectrum of as-isolated NiSOD. To achieve a satisfactory fit of these three spectra, a minimum of 11 Gaussian bands

---

(21) Becke, A. D. *J. Chem. Phys.* **1993**, *98*, 5648−5652.Becke, A. D. *J. Chem. Phys.* **1993**, *98*, 1372−1377.

(22) Lee, C. T.; Yang, W. T.; Parr, R. G. *Phys. Rev. B: Condens. Matter* **1988**, *37*, 785−789.

(23) (a) Bergman, D. L.; Laaksonen, L.; Laaksonen, A. *J. Mol. Graphics Modell.* **1997**, *15*, 301. (b) Laaksonen, L. *J. Mol. Graphics* **1992**, *10*, 33.

(24) (a) Neese, F. *J. Chem. Phys.* **2003**, *118*, 3939−3948. (b) Neese, F. *Curr. Opin. Chem. Biol.* **2003**, *7*, 125−135. (c) Neese, F. *J. Chem. Phys.* **2001**, *115*, 11080−11096.

(25) Kutzelnigg, W.; Fleischer, U.; Schindler, M. *The IGLO Method: Ab Initio Calculation and Interpretation of NMR Chemical Shifts and Magnetic Susceptibilities*; Springer-Verlag: Heidelberg, 1990; Vol. 23.

(26) (a) Ridley, J.; Zerner, M. C. *Theor. Chem. Acc.* **1973**, *32*, 111. (b) Zerner, M. C.; Loew, G. H.; Kirchner, R. F.; Mueller-Westerhof, U. T. *J. Am. Chem. Soc.* **1980**, *102*, 589.

(27) Bacon, A. D.; Zerner, M. C. *Theor. Chem. Acc.* **1979**, *53*, 21.

Table 1. Relevant Spectral Parameters for $NiSOD_{ox}$ and $NiSOD_{red}$, Obtained from Gaussian Deconvolutions of the Experimental Spectra of As-Isolated and Reduced NiSOD (Figures 1 and 2, respectively)

$NiSOD_{ox}$ band	ν_{max} (cm^{-1})	ϵ_{abs}[a] ($M^{-1}\ cm^{-1}$)	osc. str.[b] ($f_{exp} \times 10^3$)	$\Delta\epsilon$(CD)[a] ($M^{-1}\ cm^{-1}$)	$\Delta\epsilon$(MCD)[a] ($M^{-1}\ cm^{-1}$)	C_0/D_0[c]
1	14 380	300	2.8	3.7	−8.2	0.0233
2	15 650	510	4.7	4.9	5.7	0.0095
3	18 000	1340	12.3	−5.8	−34.8	0.0221
4	19 920	1510	15.1	2.0	−24.9	0.0140
5	23 290	2020	21.7	4.8	−53.7	0.0226
6	24 700	3080	33.1	24.0	−13.1	0.0036
7	26 850	6800	73.1	−14.3	−144.5	0.0181
8	28 720	4020	40.1	15.1	−20.3	0.0043
9	30 400	4900	48.9	−2.1	18.8	0.0033
10	31 950	4740	47.3	−8.0	−30.3	0.0054

$NiSOD_{red}$ band	ν_{max} (cm^{-1})	ϵ_{abs} ($M^{-1}cm^{-1}$)	osc. str.[b] ($f_{exp} \times 10^3$)	$\Delta\epsilon$(CD) ($M^{-1}\ cm^{-1}$)
A	17 110	70	0.7	1.3
B	18 430	150	1.5	2.4
C	20 500	180	1.8	−0.8
D	22 240	480	5.5	−2.6
E	24 970	500	6.5	−0.1
F	27 650	880	11.5	0.7
G	29 220	750	9.8	3.1

[a] The ϵ_{abs} and Δ_ϵ values listed pertain to $NiSOD_{ox}$ and were obtained under the assumption that as-isolated NiSOD is an equal mixture of oxidized and reduced protein. [b] $f_{exp} = (4.61 \times 10^{-9})\epsilon_{abs}\nu_{1/2}$. [c] $C_0/D_0 = (kT/\beta H)[\Delta\epsilon(MCD)/\epsilon_{abs}]$.

(dotted lines in Figure 1) of roughly equal bandwidths were needed, with peak positions and intensities as indicated in Table 1. A similar analysis was performed for the absorption and CD spectra obtained for $NiSOD_{red}$ (Figure 2), where in this case the individual bands are labeled with letters to avoid confusion (Table 1). As with the absorption data, the as-isolated CD spectrum contains contributions from both oxidized and reduced protein, although the CD features of $NiSOD_{red}$ are again considerably less intense than those of $NiSOD_{ox}$ and nearly all spectral features are attributed to the latter. Despite this, comparison of the room-temperature (rt) CD spectra of as-isolated and DTH-reduced NiSOD (Figure S2) reveals that band D of $NiSOD_{red}$ is responsible for the weak, negatively signed feature at ~22 000 cm^{-1} in the as-isolated spectrum. This assignment is corroborated by the fact that band D carries very little intensity in the corresponding MCD spectrum (Figure 1) that is dominated by features associated with the paramagnetic $NiSOD_{ox}$ species. The remaining 10 bands arise primarily from $NiSOD_{ox}$, although several contain minor contributions from $NiSOD_{red}$ transitions.[28]

All MCD band intensities increase with decreasing temperature (data not shown), characteristic of a ***C***-term mechanism and consistent with the paramagnetic nature of $NiSOD_{ox}$. Variable-temperature variable-field MCD (VTVH-MCD) data collected at 26880 cm^{-1} (Figure S3) are clearly indicative of a $S=1/2$ system, as expected given the low-spin d^7 electron configuration of the Ni^{3+} center in $NiSOD_{ox}$. As in the absorption spectrum, the most intense MCD feature is band 7, and apart from weak positive features at 15 700 and 30 400 cm^{-1} (bands 2 and 9, respectively), the spectrum consists primarily of negatively signed bands. This large imbalance between positive and negative intensity indicates that MCD signal intensity arises primarily from mixing (via spin−orbit coupling) of the ground state with low-lying excited state(s), as opposed to mixing among excited states. Compared to Cu^{2+} systems,[29] the C_0/D_0 ratios (where C_0 and D_0 are the corresponding MCD and absorption intensities, respectively) of bands 1−10 of $NiSOD_{ox}$ are somewhat small and fairly uniform in magnitude, varying by less than an order of magnitude from 0.003 to 0.023. These values suggest that the majority of bands contributing to the $NiSOD_{ox}$ absorption spectrum arise from charge transfer (CT) transitions; in this case, presumably containing significant S → Ni^{3+} character. More detailed band assignments are provided below.

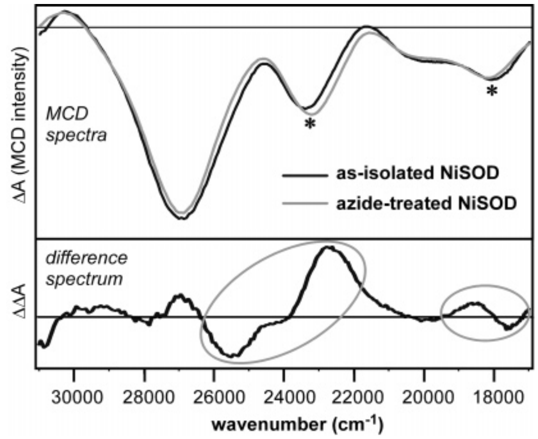

Figure 3. Top: Comparison of MCD spectra of as-isolated NiSOD (black) and NaN_3-treated (200 equiv) NiSOD (gray). Both spectra were obtained at 4 K with a magnetic field of 7 T. Peaks that shift in energy upon treatment with NaN_3 are indicated with (*). Bottom: Difference MCD spectrum obtained by subtracting the spectrum of NaN_3-treated NiSOD from that of as-isolated NiSOD. Derivative-shaped features, representing significant band shifts, are circled in gray.

The spectroscopic properties of as-isolated NiSOD were also studied in the presence of azide, a close electronic mimic of superoxide and a weak inhibitor of NiSOD.[3] Although addition of 200 equiv of NaN_3 to the as-isolated protein resulted in virtually no change of the rt absorption and CD spectra, small shifts of bands 3 and 5 are discernible in the low-temperature MCD spectra (Figure 3, top). Even though these shifts are only ~200 cm^{-1} in magnitude, they are clearly apparent in the two derivative-shaped features centered at 24 000 and 18 200 cm^{-1} in the difference spectrum shown in Figure 3, bottom. While the small magnitude of the spectral perturbations precludes the formation of a direct $Ni-N_3$ bond, our results suggest that the azide anion is capable of binding *near* the Ni^{3+} center of $NiSOD_{ox}$. This hypothesis is fully consistent with a recent EPR study carried out by Barondeau et al.,[6] where it was found that treatment of as-isolated NiSOD with azide resulted in the appearance of fine structure (due to hyperfine interactions) within the g_y resonance; however, the spectrum was unaffected by $^{14}N \rightarrow {}^{15}N$ isotopic labeling of azide, thereby arguing against the formation of an inner-sphere complex.

The rt absorption and CD spectra of $NiSOD_{red}$ (Figure 2) both exhibit two features in the visible region at ~18 000 and

---

(28) With the exception of band D, the absorption and CD bands of $NiSOD_{red}$ are not included in Figure 1, as they are very weak compared to those of $NiSOD_{ox}$. Of the eleven bands that are required by the Gaussian deconvolution, only one (band D) reflects the presence of $NiSOD_{red}$ in the sample mixture, while the others arise primarily from $NiSOD_{ox}$. For this reason, only band D of $NiSOD_{red}$ is displayed in Figure 1.

(29) (a) Solomon, E. I.; Hanson, M. A. In *Inorganic Electronic Structure and Spectroscopy*; Solomon, E. I., Lever, A. B. P., Eds.; John Wiley & Sons: New York, 1999; Vol. 2, pp 1−129. (b) Gewirth, A. A.; Solomon, E. I. *J. Am. Chem. Soc.* **1988**, *110*, 3811−3819.

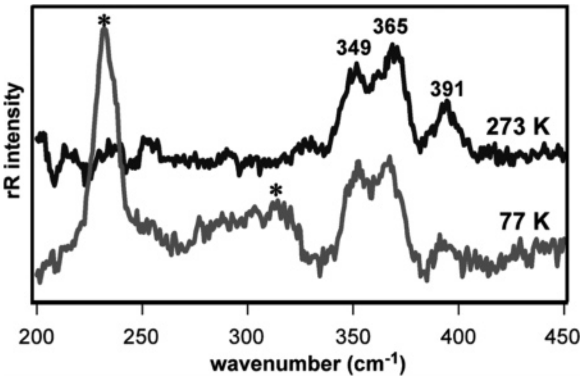

Figure 4. Resonance Raman spectra of as-isolated NiSOD obtained at 273 K (dark line, top) and 77 K (gray line, bottom). The 273 and 77 K data were obtained using 413.1 and 406.7 nm laser excitation, respectively. (*) indicates peaks arising from ice lattice modes.

21 800 cm^{-1}, along with a more intense shoulder near ∼29 000 cm^{-1}. Our spectral deconvolution (Figure 2) indicates that the low-energy features are composed of two bands each (Table 1). As noted previously, these bands are weak compared to those observed for $NiSOD_{ox}$, indicating a dramatic change in electronic structure upon metal-ion reduction. Given the results of recent structural studies,[6−8] it is not surprising that the absorption spectrum of $NiSOD_{red}$ closely resembles those reported for synthetic square-planar Ni^{2+} complexes with N_2S_2 coordination, in which the S-donor is an alkyl thiolate. For such complexes, the two weak features in the visible region are typically assigned to Ni^{2+} ligand-field (LF) transitions.[30,31] These bands appear around 16 500 and 20 500 cm^{-1} in complexes where the N-donor ligands are amines[31−35] but blue-shift to ∼18 100 and 22 700 cm^{-1} in complexes with deprotonated amides,[30,36] a direct consequence of the relative destabilization of the unoccupied Ni($x^2 - y^2$) orbital caused by the greater donor strength of the latter ligands. The corresponding band energies for $NiSOD_{red}$ are intermediate between these two sets, in agreement with the fact that the active site contains a mixed ligation consisting of a neutral amine and a deprotonated amide.

Figure 4 shows the rR spectra of as-isolated NiSOD obtained at 273 and 77 K using 413 and 407 nm excitation, respectively. Although these data are of reasonable quality, our rR studies were complicated by the fact that the major absorption feature of NiSOD lies in the near-UV region, which forced us to use laser excitation wavelengths that were somewhat off-resonance. Nonetheless, three protein-derived vibrational features are clearly observed at 349, 365, and 391 cm^{-1}, with the first two peaks carrying much more intensity than the third (Figure 4).

Upon examination of the $NiSOD_{ox}$ active-site structure, it is reasonable to assign the 349 and 365 cm^{-1} peaks to the Ni^{3+}−S based stretching modes, ν(Ni−S), involving the Cys2 and Cys6 residues. These assignments are supported by the fact that the sample peaks are strongly enhanced by excitation into the onset of the dominant NiSOD absorption feature at ∼27 000 cm^{-1}, which arises primarily from S → Ni^{3+} CT transitions (vide infra), whereas spectra obtained with lower-energy light (i.e., 488 nm excitation) lacked these features. The higher-energy peak at 391 cm^{-1} may arise from a mode involving both Ni−S stretching and S−C_β−C_α−N bending motions of the Cys2 backbone as a result of strong kinematic coupling. Alternatively, this peak might also be due to the ν(Ni−N(Cys2)) mode, which could be enhanced in response to the electronic changes at the Ni center accompanying CT excitation.

Table 2. Relevant Interatomic Distances (Å) for DFT-Optimized Models of NiSOD and Comparison to Crystallographic Data

	DFT			X-ray Structure	
$NiSOD_{ox}$	ox^1	ox^2	ox^3	1T6U[f]	1Q0G[g]
$Ni-N_{ax}$[a]	2.07	2.14	2.16	2.35	2.63
$Ni-N(His1)_{eq}$[b]	2.03	2.01	2.02	2.02	2.11
$Ni-N(Cys2)_{eq}$[c]	1.93	1.91	1.91	1.91	1.93
$Ni-S_2$[d]	2.18	2.19	2.17	2.16	2.24
$Ni-S_6$[e]	2.24	2.25	2.25	2.19	2.26

	DFT			X-ray structure	
$NiSOD_{red}$	red	red-S_2H	red-S_6H	1T6U[f]	1Q0D[g]
$Ni-N_{ax}$[a]	3.98	3.88	3.82	4.26	3.81
$Ni-N(His1)_{eq}$[b]	1.99	1.96	1.99	1.87	2.07
$Ni-N(Cys2)_{eq}$[c]	1.89	1.89	1.86	1.91	1.94
$Ni-S_2$[d]	2.18	2.15	2.18	2.16	2.24
$Ni-S_6$[e]	2.22	2.21	2.19	2.19	2.18

[a] N_{ax} = coordinating N of the axial imidazole ligand. [b] $N(His1)_{eq}$= equatorial N ligand of the His1 residue. [c] $N(Cys2)_{eq}$ = equatorial N ligand of the Cys2 residue. [d] S_2 = S ligand of the Cys2 residue. [e] S_6 = S ligand of the Cys6 residue. [f] From ref 6. [g] From ref 7.

Computational Results. (a) Active-Site Models. Using the recent X-ray crystal structures as a starting point, active-site models of NiSOD in both the oxidized and reduced states were generated using DFT geometry optimizations (see Experimental Section for details). Our initial models, referred to as $\mathbf{ox^1}$ and **red**, included only the first-sphere residues His1, Cys2, and Cys6 (Figure 5). Relevant bond lengths of the optimized $\mathbf{ox^1}$ and **red** models are provided in Table 2, along with the corresponding crystallographic data (see Table S1 for additional structural parameters). The $\mathbf{ox^1}$ and **red** models clearly reproduce the coordination geometry of the equatorial ligands quite well, generally providing bond distances within 0.05 Å of the experimental values.[6,7] However, DFT predicts an axial $Ni-N_{ax}$ distance (2.07 Å) that is much shorter than the crystallographically determined distance (≥2.3 Å), although the computational value is entirely consistent with Ni−imidazole bond lengths in synthetic complexes.[6,37] As the His1 residue could potentially function in proton transfer to the substrate $O_2^{\bullet-}$ (similar to the putative role played by the bridging His residue in Cu/ZnSOD[11]), we also computed the active-site structure assuming an axial imidazol*ate* ligand (model $\mathbf{ox\text{-}His_{dep}}$). Interestingly, the resulting structure is nearly identical to that of $\mathbf{ox^1}$ but, not unexpectedly, features an even shorter (by 0.03 Å) $Ni-N_{ax}$ bond distance.

Structural studies of NiSOD have revealed hydrogen-bonding interactions between the imidazole moiety of His1 and several second-sphere residues, such as Glu17, Arg47, and Val8.[6,7] To

---

(30) Kruger, H. J.; Peng, G.; Holm, R. H. *Inorg. Chem.* **1991**, *30*, 734−742.
(31) Maroney, M. J.; Choudhury, S. B.; Bryngelson, P. A.; Mirza, S. A.; Sherrod, M. J. *Inorg. Chem.* **1996**, *35*, 1073−1076.
(32) Colpas, G. J.; Kumar, M.; Day, R. O.; Maroney, M. J. *Inorg. Chem.* **1990**, *29*, 4779−4788.
(33) (a) Mills, D. K.; Reibenspies, J. H.; Darensbourg, M. Y. *Inorg. Chem.* **1990**, *29*, 4364−4366. (b) Farmer, P. J.; Reibenspies, J. H.; Lindahl, P. A.; Darensbourg, M. Y. *J. Am. Chem. Soc.* **1993**, *115*, 4665−4674.
(34) Smee, J. J.; Miller, M. L.; Grapperhaus, C. A.; Reibenspies, J. H.; Darensbourg, M. Y. *Inorg. Chem.* **2001**, *40*, 3601−3605.
(35) Grapperhaus, C. A.; Maguire, M. J.; Tuntulani, T.; Darensbourg, M. Y. *Inorg. Chem.* **1997**, *36*, 1860−1866.
(36) Hanss, J.; Kruger, H. J. *Angew. Chem., Int. Ed.* **1998**, *37*, 360−363.
(37) See, R. F.; Kruse, R. A.; Strub, W. M. *Inorg. Chem.* **1998**, *37*, 5369−5375.

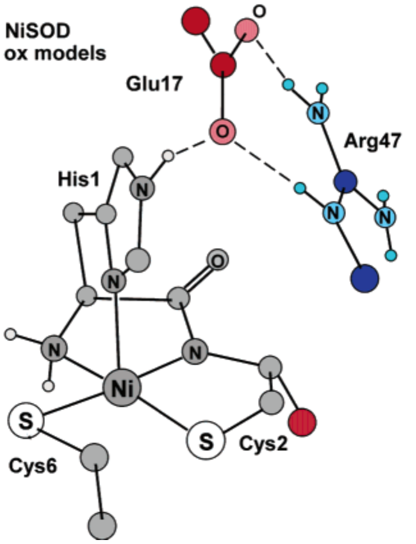

Figure 5. Illustration of the various computational models of oxidized NiSOD. The **ox^1** model (gray) includes the Ni center and the first-sphere ligands from His1, Cys2, and Cys6. The larger **ox^2** model (gray + red + blue) contains the carboxylate group of Glu17 and the positively charged guanidino group of Arg47, while **ox^3** (gray + red) lack the latter. Both **ox^2** and **ox^3** also possess an additional $-CH_3$ group derived from Cys2. The dotted lines reflect hydrogen bonding interactions. All unlabled atoms are either carbons (large) or hydrogens (small). Note that, for clarity, only a subset of the hydrogen atoms used in the computational models is shown here.

model these interactions, we also performed DFT optimizations on active-site models that included the side chains of certain second-sphere residues. Model **ox^2** features both the carboxylate group of Glu17 and the positively charged guanidino group of Arg47, while **ox^3** includes only the former (Figure 5). The positions of these additional residues were constrained so as to prevent geometries incompatible with the restricted flexibility of the protein backbone. In the resulting optimized structures, the strong hydrogen-bonding interaction between the (Glu17)$-CO_2^-$ and (His1)N$-$H units causes a lengthening of the axial Ni$-N_{ax}$ bond by nearly 0.10 Å. Since the presence of Arg47 reduces the hydrogen-bond accepting ability of Glu17, the Ni$-N_{ax}$ bond elongation is more dramatic for **ox^3** than for **ox^2**, yet even the distance of 2.16 Å in the former model remains significantly shorter than the experimental value. This discrepancy suggests that either (i) our truncated active-site models fail to account for all steric and/or electronic forces or (ii) the Ni$-N_{ax}$ distance found experimentally is artificially large due to the redox heterogeneity of the crystals used in the X-ray structural studies. Regardless, our results clearly demonstrate that second-sphere residues, particularly Glu17, influence the position of the His1 imidazole group, having profound implications for the electronic properties of NiSOD$_{ox}$ (vide infra).

It has been suggested that the coordinated thiolates in NiSOD could function in proton transfer to the nascent peroxide O_2^{2-} following substrate reduction (eq 1b).[8,9] To examine this hypothesis, DFT optimizations were performed on two additional models, **red-S$_2$H** and **red-S$_6$H**, in which the Cys2 and Cys6 residues, respectively, of NiSOD$_{red}$ were converted to thiols. As shown in Table 2, in both models the Ni$-$S bond distances actually *shortened* slightly upon protonation, while the other Ni$-$ligand bond distances remained largely unaffected. This finding, while somewhat counterintuitive, concurs nicely with previous synthetic and computational studies of $Ni^{2+}S_xN_y$ complexes, which revealed only modest changes in Ni$-$S bond distances upon protonation,[38] alkylation,[33,39,40] or oxidation[34,35,41-43] of the coordinated thiolate(s). A rationale for these structural changes (or lack thereof) is presented below. Importantly, our calculations demonstrate that the Cys2 and Cys6 residues are capable of binding H$^+$ without significantly distorting the active-site geometry.

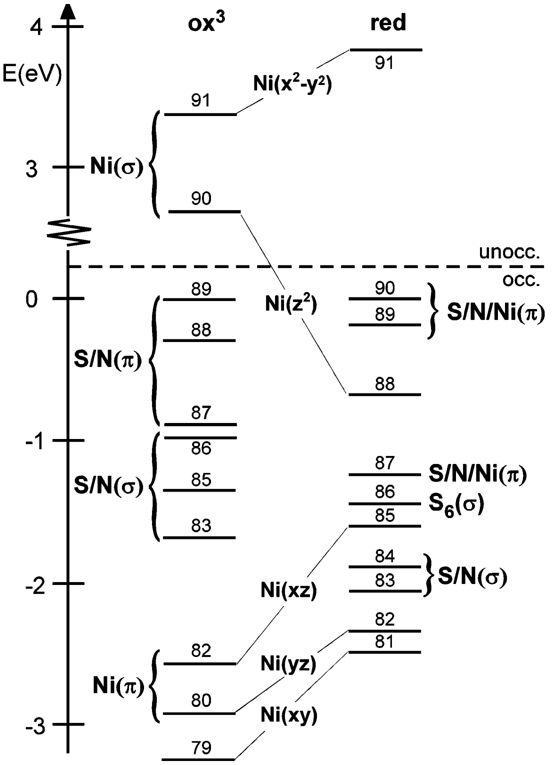

Figure 6. MO energy diagrams for oxidized and reduced NiSOD obtained from DFT calculations of the **ox^3** and **red** models, respectively. For **ox^3**, only the spin-down MOs from the unrestricted calculation are displayed. The MOs are arranged in energy relative to the corresponding HOMO and labeled according to their principal contributors (see Tables 3 and 4 for more information).

(b) Bonding Descriptions of NiSOD. To further probe the electronic structure of the NiSOD active site, spin-unrestricted single-point DFT calculations utilizing the B3LYP hybrid functional were performed on models **ox^1** and **ox^3**, while spin-restricted calculations were carried out for the **red** model. Tables 3 and 4 summarize the energies and compositions of relevant molecular orbitals (MOs) of **ox^3** and **red**, respectively, and the corresponding MO energy-level diagrams are shown in Figure 6. For the **ox** models, spin-polarization lowers the energies of the majority-spin (i.e., spin-up) Ni d orbitals relative to their

---

(38) Allan, C. B.; Davidson, G.; Choudhury, S. B.; Gu, Z. J.; Bose, K.; Day, R. O.; Maroney, M. J. *Inorg. Chem.* **1998**, *37*, 4166−4167.

(39) Fox, D. C.; Fiedler, A. T.; Halfen, H. L.; Brunold, T. C.; Halfen, J. A. *J. Am. Chem. Soc.* **2004**, *126*, 7627−7638.

(40) Bellefeuille, J. A.; Grapperhaus, C. A.; Derecskei-Kovacs, A.; Reibenspies, J. H.; Darensbourg, M. Y. *Inorg. Chim. Acta* **2000**, *300*, 73−81.

(41) (a) Mirza, S. A.; Pressler, M. A.; Kumar, M.; Day, R. O.; Maroney, M. J. *Inorg. Chem.* **1993**, *32*, 977−987. (b) Kumar, M.; Colpas, G. J.; Day, R. O.; Maroney, M. J. *J. Am. Chem. Soc.* **1989**, *111*, 8323−8325. (c) Mirza, S. A.; Day, R. O.; Maroney, M. J. *Inorg. Chem.* **1996**, *35*, 1992−1995.

(42) (a) Grapperhaus, C. A.; Darensbourg, M. Y. *Acc. Chem. Res.* **1998**, *31*, 451−459. (b) Grapperhaus, C. A.; Mullins, C. S.; Kozlowski, P. M.; Mashuta, M. S. *Inorg. Chem.* **2004**, *43*, 2859−2866.

(43) Kaasjager, V. E.; Bouwman, E.; Gorter, S.; Reedijk, J.; Grapperhaus, C. A.; Reibenspies, J. H.; Smee, J. J.; Darensbourg, M. Y.; Derecskei-Kovacs, A.; Thomson, L. M. *Inorg. Chem.* **2002**, *41*, 1837−1844.

Table 3. Energies and Compositions (%) of Relevant Spin-Down Molecular Orbitals of Model **ox^3** as Obtained from a Spin-Unrestricted DFT Calculation

MO [a]	*E* (eV)	Ni [b]	N_{ax} [c]	$N(His1)_{eq}$ [d]	N/O(Cys2) [e]	S_2 [f]	S_6 [g]	orbital composition
Unoccupied								
91	−1.88	49.2	0.2	5.5	7.7	15.5	14.1	$Ni(x^2 - y^2)$
90	−2.61	75.7	6.1	1.6	1.9	7.7	1.3	$Ni(z^2)$
Occupied								
89	−5.30	5.3	0.5	0.7	0.8	14.8	69.0	$S_6(\pi)$
88	−5.62	9.6	0.4	0.1	33.1	39.8	3.6	$S_2(\pi) + N/O(\pi)$
87	−6.24	7.6	0.4	0.4	51.6	15.3	11.9	$N/O(\pi) + S_2(\pi) + S_6(\pi)$
86	−6.33	8.7	0.1	1.0	51.2	8.7	14.4	$N/O(\sigma) + S_6(\sigma)$
85	−6.72	12.5	0.1	1.0	22.6	1.3	42.1	$S_6(\sigma) + N/O(\sigma)$
83	−7.09	16.8	0.5	5.4	0.7	53.8	7.2	$S_2(\sigma)$
82	−8.00	47.2	5.3	0.2	3.8	3.6	11.9	$Ni(xz)$
80	−8.39	52.1	13.7	0.0	3.0	2.0	2.9	$Ni(yz)$
79	−8.72	62.3	3.1	3.0	7.1	3.1	2.3	$Ni(xy)$

[a] MOs 84 and 81 were not included because they are ligand-based and do not participate in Ni-ligand bonding interactions. [b] Ni 3d, 4s, and 4p contributions. [c] 2s and 2p contributions from the coordinating N atom of the axial imidazole ligand. [d] 2s and 2p contributions from the equatorial N ligand from the amine group of His1. [e] 2s and 2p contributions from the N and O atoms of the Cys2 residue. [f] S 3s, 3p, and 3d contributions from the Cys2 residue. [g] S 3s, 3p, and 3d contributions from the Cys6 residue.

Table 4. Energies and Compositions (%) of Relevant Molecular Orbitals of Model **red** as Obtained from a Spin-Restricted DFT Calculation

MO	*E* (eV)	Ni [a]	$N(His1)_{eq}$ [b]	N/O(Cys2) [c]	S_2 [d]	S_6 [e]	orbital composition
Unoccupied							
91	2.68	42.5	4.5	4.4	11.9	8.6	$Ni(x^2 - y^2)$
Occupied							
90	−1.12	24.9	0.3	1.2	28.7	38.2	$S_2(\pi) + S_6(\pi) + Ni(xz/yz)$
89	−1.33	36.9	0.1	10.5	32.4	11.8	$S_2(\pi) + N/O(\pi) + Ni(xz/yz)$
88	−1.80	90.4	0.7	1.0	3.2	2.5	$Ni(z^2)$
87	−2.35	32.6	1.1	21.2	4.7	31.4	$S_6(\pi) + N/O(\pi) + Ni(yz)$
86	−2.57	15.4	1.1	18.5	4.7	49.3	$S_6(\sigma)$
85	−2.77	53.0	1.5	2.8	29.1	6.4	$Ni(xz)$
84	−3.05	38.3	2.2	1.4	39.6	10.1	$S_2(\sigma)$
83	−3.13	8.2	0.8	63.9	2.1	5.3	$N/O(\sigma)$
82	−3.47	38.1	0.1	40.9	2.6	3.3	$Ni(yz) + N/O(\pi)$
81	−3.62	69.2	1.1	2.6	11.5	4.0	$Ni(xy)$

[a] Ni 3d, 4s, and 4p contributions. [b] 2s and 2p contributions from the equatorial N ligand from the amine group of His1. [c] 2s and 2p contributions from the N and O atoms of the Cys2 residue. [d] S 3s, 3p, and 3d contributions from the Cys2 residue. [e] S 3s, 3p, and 3d contributions from the Cys6 residue.

minority-spin (i.e., spin-down) counterparts, resulting in substantial mixing of the former with ligand-based orbitals. For this reason, Table 3 includes only the spin-down ligand- and Ni d-based MOs that are considerably less mixed, and thus easier to analyze, than their spin-up counterparts.

The composition of the lowest-energy unoccupied spin-down MO (#90) of **ox^3** indicates that the lone unpaired electron of NiSOD resides in a Ni(z^2)-based MO (Figure 7a and Table 3), in agreement with previous EPR results. Moreover, the substantial N_{ax} character (6%) computed for this MO provides a rationale for the large nitrogen hyperfine coupling ($A_{zz} = 69.7$ MHz) observed experimentally.[8] Comparison of the DFT results for models **ox^1** and **ox^3** reveals that elongation of the Ni−N_{ax} bond from 2.07 to 2.16 Å lowers the energy of the Ni(z^2)-based MO by 0.23 eV while leaving the energies and compositions of the remaining MOs virtually unchanged. As expected for this distorted square-pyramidal active site, the unoccupied Ni($x^2 - y^2$)-based MO (#91) lies at higher energy. The large destabilization of the Ni($x^2 - y^2$)-based MO relative to the other Ni d-based MOs is primarily due to covalent σ-bonding interactions between Ni and the two cysteine residues, with the nitrogen donors contributing to a lesser extent (Table 3).

While the two lowest-energy unoccupied spin-down MOs of **ox^3** have primarily Ni character, the six highest-energy occupied MOs are predominately ligand-centered, lying well above the set of three occupied Ni d-based MOs (Figure 6 and Table 3). These ligand-based MOs are highly mixed, possessing contributions from three of the four equatorial ligands, namely, the two thiolates (Cys2 and Cys6) and the deprotonated amide unit that donates from both its N and O atoms. The bonding interactions between Ni^{3+} and the two S 3p-based lone pairs of each cysteine residue are primarily determined by the corresponding Ni−S−C_β bond angles,[44] which have values of 95° and 114° for Cys2 and Cys6, respectively (Scheme 2). As these angles are much closer to 90° than 180°, both thiolates possesses a σ- and a π-donating lone pair (S(σ) and S(π), respectively), and the orientation of the two thiolates with respect to the other active-site ligands ensures that the two S(π) orbitals are aligned with the axial z-direction (Scheme 2). Similarly, the deprotonated amide group also functions as an effective σ- and π-donor, where, again, the π-interaction involves a ligand orbital whose lobes are oriented parallel to the z-axis. Due to π-conjugation, the amide-based MOs carry considerable amounts of orbital character from both the nitrogen and the carbonyl oxygen. As indicated in Figure 6, the π-donor orbitals from the equatorial ligands are the dominant contributors to the three highest-energy MOs (#89−87), while the corresponding σ-donor based MOs are lower in energy (#86−85, 83). Given the orientation of the ligand π-donor orbitals along the molecular z-axis, it is not surprising that the Ni^{3+} d-orbital splitting pattern places the Ni(π)-based MOs (#82, 80) higher in energy than the Ni(xy)-based MO (#79). In general, the Ni^{3+}-ligand bonding interactions are moderately covalent, with an average of 25% S/N/O

Scheme 2. Schematic Illustration of Ligand Frontier Orbitals Involved in Bonding to the Ni Center

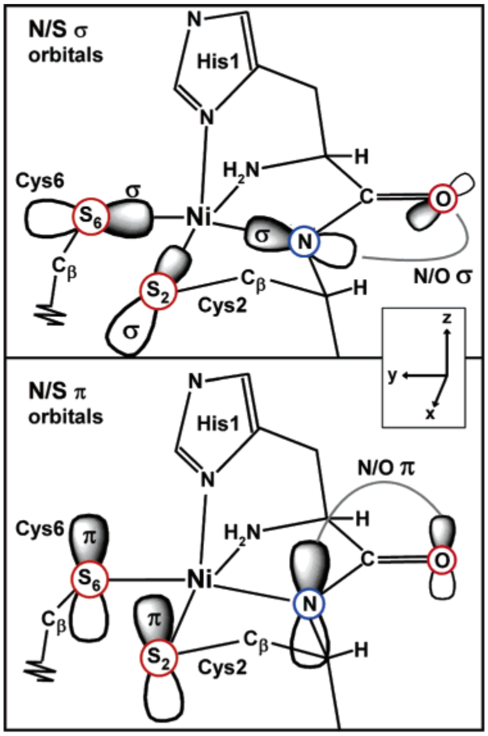

orbital character in the Ni d-based MOs and 10% Ni orbital character in the ligand-based MOs.

Reduction of the active site from $Ni^{3+} \rightarrow Ni^{2+}$ (**ox^3** → **red**) alters the bonding scheme described above in two significant ways: (i) dissociation of the axial imidazole ligand strongly stabilizes the Ni(z^2)-based MO relative to the other MOs, and (ii) the reduced positive charge on the metal center destabilizes the Ni(π) set of orbitals, diminishing their energy separation from the ligand frontier orbitals (Figure 6). This reduction in energy splitting leads to extensive mixing between these two sets of orbitals, and the resulting MOs reveal a high degree of metal−ligand bond covalency, making it difficult to distinguish between Ni- and ligand-based MOs. It should be noted that the bonding scheme developed for **red** is not unique to NiSOD$_{red}$, as previous studies of Ni−thiolate interactions in synthetic[40,42] and biological[45] systems have yielded similarly covalent metal−ligand bonding descriptions. As shown in Figure 7b, the two highest-energy occupied MOs of **red** (#90 and 89) reveal strongly covalent π-antibonding interactions between the Ni(π) orbitals and the π-donor orbitals of the equatorial ligands, with ~30% Ni and 60% ligand orbital character (Table 4). In contrast to the situation found for the **ox** models, these Ni/S/N-derived MOs with π-symmetry are now higher in energy than the Ni(z^2)-based MO of **red** by ~4500 cm^{-1}.

To better characterize the redox-active orbital of NiSOD$_{red}$, model **red** was oxidized by one electron and reoptimized, which yielded the square-planar Ni^{3+} model **ox-His$_{off}$** that is isoelectronic with the **ox$^{1-3}$** models but lacks the Ni−N$_{ax}$ bonding interaction. The structure of **ox-His$_{off}$** is nearly identical to that of **red**, although the Ni−S$_6$ bond distance is shorter by 0.08 Å. As shown in Figure 7c, the extra "hole" resulting from one-electron oxidation of **red** resides in a π-type MO comprised of the following orbitals: 58% Ni(yz), 24% S$_6$(π), and 10% N/O(π). Thus, while the HOMO of **red** is largely thiolate-based (66%), the "redox active" MO of **ox-His$_{off}$** is primarily Ni d-based, consistent with a Ni^{3+} description of this model. In support of a metal-centered **red** → **ox-His$_{off}$** oxidation, the calculated Mulliken populations reveal that 70% of the unpaired spin of **ox-His$_{off}$** is localized on Ni. Thus, despite the high metal−ligand bond covalency found for the **red** model of NiSOD$_{red}$, our results suggest that the enzyme active site has evolved such as to allow for metal-based oxidation by destabilizing the Ni(π) orbital(s) via strong Ni−ligand π−antibonding interactions. Moreover, our DFT results suggest that the redox-active MO for NiSOD is different in the two half-reactions, being Ni(z^2)-based for $O_2^{\bullet -}$ oxidation (eq 1a) and Ni/S/N(π)-based for $O_2^{\bullet -}$ reduction (eq 1b). Note that this scenario is based on the assumption that in the substrate reduction step the imidazole group of His1 remains dissociated and coordinates to Ni after, rather than concomitant with, metal-ion oxidation, which seems reasonable considering that in this case electron transfer presumably occurs on a much faster time scale than nuclear motions.

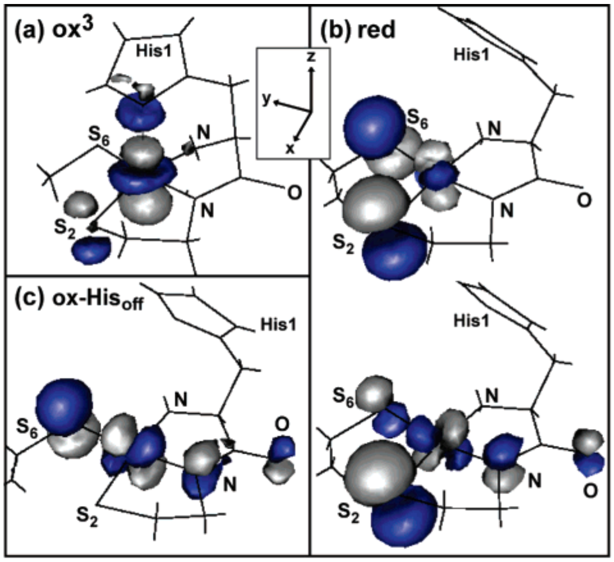

Figure 7. DFT-generated isosurface plots of (a) the spin-down LUMO of model **ox^3** (#90), (b) the two highest-energy occupied MOs of model **red** (#90 and 89, top and bottom, respectively), and (c) the spin-down LUMO of model **ox-His$_{off}$**.

(c) Comparison to Synthetic [NiS$_2$N$_2$] Complexes. The active site of NiSOD$_{red}$ bears a close resemblance to a family of synthetic $Ni^{2+}S_2N_2$ complexes that have been prepared over the past two decades.[30−35,42,43] Based on the identity of the nitrogen ligands, these complexes can be divided into two classes: (i) neutral complexes with two amine ligands and (ii) dianionic complexes with two deprotonated amide ligands, represented by [Ni(dmpn)]^0 (**1**) and [Ni(ema)]$^{2-}$ (**2**), respectively, in Scheme 3 (dmpn is the dianion of *N*,*N*′-dimethyl-*N*,*N*′-bis(2-mercaptoethyl)-1,3-propanediamine and ema is the tetraanion of *N*,*N*′-ethylenebis(2-(mercapto)acetamide)). Ni−thiolate complexes with neutral N-donor ligands, like **1**, react with O_2 at sulfur to yield coordinated sulfonate ligands.[35,41−43] Significantly, 1e$^-$ oxidation of these complexes is

---

[44] Solomon, E. I.; Szilagyi, R. K.; George, S. D.; Basumallick, L. *Chem. Rev.* **2004**, *104*, 419−458.

[45] (a) Craft, J. L.; Horng, Y. C.; Ragsdale, S. W.; Brunold, T. C. *J. Am. Chem. Soc.* **2004**, *126*, 4068−4069. (b) Craft, J. L.; Horng, Y. C.; Ragsdale, S. W.; Brunold, T. C. *J. Biol. Inorg. Chem.* **2004**, *9*, 77−89.

Scheme 3

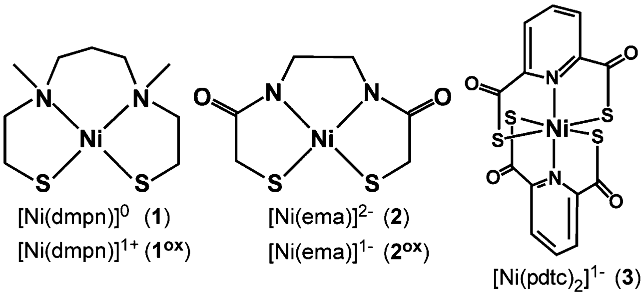

Table 5. Compositions of “Redox-Active” Molecular Orbitals and Mulliken Spins Obtained from DFT Calculations on NiSOD Models and Synthetic Complexes **1** and **2**

			MO composition (%)			Mulliken spin	
			Ni[a]	S[b]	N[c]	Ni	S
[Ni(dmpn)]	**1**	HOMO	16.5	76.8	0.0		
		HOMO-1	35.2	57.6	0.1		
	1^{ox}	SOMO[d]	25.4	68.4	0.0	0.25	0.74
[Ni(ema)]	**2**	HOMO	36.0	54.2	3.4		
		HOMO-1	43.2	37.4	14.2		
	2^{ox}	SOMO[d]	59.1	26.8	8.0	0.67	0.24
NiSOD	**red**	HOMO	26.0	66.0	1.3		
		HOMO-1	36.1	44.5	11.0		
	ox-His$_{off}$	SOMO[d]	58.2	24.8	10.3	0.70	0.24

[a] Ni 3d, 4s, and 4p contributions. [b] S 3s, 3p, and 3d contributions from both thiolates. [c] N 2s and 2p contributions from both N-donor ligands. [d] Refers to the spin-down (β) LUMO.

Table 6. Calculated EPR Parameters for $[Ni(pdtc)_2]^{1-}$ and NiSOD **ox** Models

		g-values			N_{ax} hyperfine splitting (MHz)		
EPR parameters		g_x	g_y	g_z	A_{xx}	A_{yy}	A_{zz}
$Ni(pdtc)_2{}^{1-}$ (**3**)	expmt[b]	2.137		2.038	45.3		59.1
	DFT	2.119		2.052	47.1		59.4
	% Δ[a]	−13%			+4%		+1%
NiSOD$_{ox}$	expmt[c]	2.304	2.248	2.012	NA	NA	69.7
ox^1	DFT	2.228	2.205	2.044	50.9	52.1	64.2
	% Δ[a]	−25%	−18%				−8%
ox-His$_{dep}$	DFT	2.188	2.175	2.048	52.3	54.2	72.8
	% Δ [a]	−39%	−30%				+ 4%
ox^3	DFT	2.258	2.222	2.041	51.6	52.6	64.1
	% Δ[a]	−15%	−11%				−8%

[a] For *g*-values, $\%\Delta = 100 \times [g(\mathrm{DFT}) - g(\mathrm{expmt})]/[g(\mathrm{expmt}) - 2.003]$. For A_{zz}, $\%\Delta = 100 \times [A(\mathrm{DFT}) - A(\mathrm{expmt})]/[A(\mathrm{expmt})]$. [b] From ref 48. [c] From ref 8. NA = Not available.

irreversible and typically leads to sample decomposition via disulfide production.[32,46] These results indicate that $[NiS_2N_2]^0$ complexes have a propensity to undergo oxidation at the thiolate ligands, not at the Ni center. In contrast, $[NiS_2N_2]^{2-}$ complexes with aliphatic thiolates and aryl thiolates exhibit reversible oxidation at potentials of approximately −300 mV and 0 mV (vs SCE), respectively.[30] Yet the resulting Ni^{3+} complexes are somewhat unstable in solution,[30] and only a single $[Ni^{3+}S_2N_2]^{1-}$ complex with alkyl thiolates has been isolated to date.[36]

These studies of relevant $[NiS_2N_2]$ complexes raise important questions with respect to the structure and function of NiSOD; namely, how does the enzyme avoid sulfur-based oxidation and how can it stabilize the Ni^{3+} oxidation state? To explore these issues computationally, B3LYP DFT studies were performed on the Ni^{2+} complexes **1** and **2**, as well as their hypothetical Ni^{3+} derivatives **1^{ox}** and **2^{ox}**. Table 5 provides a summary of key results obtained for these models and the NiSOD models **red** and **ox-His$_{off}$**. The two highest-energy occupied MOs of **1** are ∼70% S(π)-based, and oxidation produces a species (**1^{ox}**) that contains a sulfur-based radical delocalized over the two thiolate ligands, in full agreement with the experimental findings described above. Exchanging the neutral amine ligands for anionic amides (**1** → **2**) results in more Ni^{2+} d-orbital character (∼40%) in the two highest-energy occupied MOs. As a result, the corresponding oxidized species (**2^{ox}**) possesses a redox-active orbital that is primarily localized on Ni (∼60%), which also carries 70% of the spin density (Table 5). Clearly, the incorporation of two anionic amide ligands stabilizes the Ni^{3+} state, leading to (mostly) metal-based oxidation. Nevertheless, the redox-active MO of model **2** possesses a considerable degree of S(π)-orbital character (∼30−40%), which likely explains the relative instability of $[Ni^{3+}S_2N_2]^{1-}$ complexes in solution.

Of particular relevance to NiSOD is the comparison of models **2** and **2^{ox}** to the corresponding NiSOD models **red** and **ox-His$_{off}$**, respectively. Interestingly, although the NiSOD$_{red}$ active site has only one anionic nitrogen ligand, our computational data suggest that it is similar to **2** in its ability to undergo metal-based oxidation (Table 5). It thus appears that one anionic amide ligand is sufficient to avoid S-centered oxidation in $[NiS_2N_2]$ systems, likely because the Ni-based redox-active MO of **ox-His$_{off}$** is oriented along the S_6−Ni−N(Cys2) bond vector (Figure 7c) and interacts with only a single N donor. The implications of these findings are further explored in the Discussion section.

(d) EPR Calculations. The calculation of EPR *g*-values and nitrogen hyperfine parameters with DFT has proven to be a valuable method for evaluating the validity of computational models on the basis of experimental data.[47] To explore the effects of structural and electronic variations on the magnetic parameters of NiSOD$_{ox}$, we performed EPR calculations for several Ni^{3+}-bound active site models utilizing the B3LYP functional. Additional computations were performed on the well-characterized complex $[Ni(pdtc)_2]^{1-}$ (**3**),[48] where pdtc = pyridine-2,6-bis(monothiocarboxylate)$^{2-}$ (Scheme 3), to gauge the ability of our methodology to accurately calculate EPR parameters for Ni^{3+} systems with N/S ligation. The calculations described herein employed the coupled-perturbed SCF (CP-SCF) equations to account for spin−orbit coupling (SOC) and magnetic field effects, an approach that has been used successfully by Neese in computational studies of complexes with first-row transition metals, including Ni.[24]

As shown in Table 6, the parameters obtained from EPR calculations on **3** indicate that the CP-SCF DFT methodology indeed provides reasonable results for Ni^{3+} systems. Specifically, the calculated nitrogen hyperfine values are nearly identical to the experimental values, and the computed *g*-values also agree fairly well with the EPR results.[48] DFT underestimates the $g_{x,y}$-shifts of **3** by 18 ppt (13%), while the g_z-shift is slightly

---

(46) (a) Kruger, H. J.; Holm, R. H. *Inorg. Chem.* **1989**, *28*, 1148−1155. (b) Nakabayashi, Y.; Masuda, Y.; Sekido, E. *J. Electroanal. Chem. Interfacial Electrochem.* **1986**, *205*, 209−218.

(47) (a) Stich, T. A.; Buan, N. R.; Brunold, T. C. *J. Am. Chem. Soc.* **2004**, *126*, 9735−9749. (b) Foerster, S.; Stein, M.; Brecht, M.; Ogata, H.; Higuchi, Y.; Lubitz, W. *J. Am. Chem. Soc.* **2003**, *125*, 83−93. (c) Stadler, C.; Lacey, A. L.; Montet, Y.; Volbeda, A.; Fontecilla-Camps, J. C.; Conesa, J. C.; Fernandez, V. M. *Inorg. Chem.* **2002**, *41*, 4424−4434. (d) Stein, M.; van Lenthe, E.; Baerends, E. J.; Lubitz, W. *J. Am. Chem. Soc.* **2001**, *123*, 5839−5840.

(48) Kruger, H. J.; Holm, R. H. *J. Am. Chem. Soc.* **1990**, *112*, 2955−2963.

overestimated by 14 ppt (40%). A similar pattern was found for the **ox^1** model; namely, the calculation yields g_x and g_y values of 2.228 and 2.205 that are smaller than the experimental values, while the corresponding g_z value of 2.044 is too large. However, the absolute and relative errors in the calculated g_x- and g_y-values are much greater for **ox^1** than **3**, suggesting a discrepancy between the geometric structures of **ox^1** and the NiSOD$_{ox}$ active site. The **ox-His$_{dep}$** model provides even worse agreement with the experimental values, suggesting that the axial ligand to the Ni^{3+} center of NiSOD$_{ox}$ is a neutral imidazole and not an anionic imidazolate. In contrast, the g-values predicted for **ox^3** are much more consistent with the experimental data, and the relative errors are comparable to those found for complex **3** (Table 6). These results reveal a close relationship between the length of the Ni−N$_{ax}$ bond and the computed g-values for NiSOD$_{ox}$. As described above, elongation of this bond reduces the energy gap between the singly occupied Ni(z^2)-based MO and the doubly occupied set of Ni-based MOs, which, in turn, increases the **g**-tensor anisotropy by promoting orbital mixing (via SOC). On the other hand, deprotonation of the axial imidazole increases this ligand's donor strength and destabilizes the Ni(z^2)-based MO, thus causing the g_x and g_y values to shift closer to the free-electron value ($g_e = 2.003$). Interestingly, the three computational models of NiSOD$_{ox}$ provide very similar values of A_{zz}, and all agree reasonably well with the experimental value of 69.7 MHz (Table 6).[49] This similarity is due primarily to the fact that, while the position and protonation state of His1 have a large effect on the energy of the Ni(z^2)-based MO, their influence on the composition of this orbital is quite small.

Spectral Assignments. The DFT-derived bonding descriptions of oxidized and reduced NiSOD presented above provide a suitable starting point for assigning key features in the corresponding absorption, CD, and MCD spectra. To assist in this endeavor, semiempirical INDO/S-CI calculations were also performed on our active-site models.

(a) Oxidized NiSOD. As shown in Figure S4, the INDO/S-CI computed spectra for the **ox^1** and **ox^3** models adequately reproduce the relative energies and intensities of key features of the as-isolated NiSOD absorption spectrum; namely, the intense band in the near-UV region accompanied by less intense shoulders to lower energy. The INDO/S-CI results also provide information regarding the nature of the electronic transitions, expressing each as a linear combination of one-electron excitations between occupied (donor) orbitals and unoccupied (acceptor) orbitals. Due to the highly mixed character of the ligand-based MOs, the donor orbitals contain sizable contributions from multiple ligands, and it is not possible to provide unambiguous transition assignments for all bands 1−10. Despite this difficulty, the results for both **ox^1** and **ox^3** clearly indicate that the three bands that comprise the intense near-UV feature at ~27 000 cm^{-1} (bands 6−8) arise mainly from S/N(σ) → Ni($x^2 - y^2$) ($\sigma \rightarrow \sigma^*$) CT transitions. More specifically, the donor orbital of the most intense transition in the absorption spectrum (band 7) has primarily S$_6$(σ) character and corresponds to MO #85 in Figure 6 and Table 3. Bands 6 and 8, which bracket this dominant feature, are then assigned to N/O(σ) → Ni($x^2 - y^2$) and S$_2$(σ) → Ni($x^2 - y^2$) CT transitions, respectively (Table 7). Based on our computational data, most of the weaker absorption features observed between 17 000 and 24 000 cm^{-1} are attributed to S/N(π) → Ni^{3+} CT transitions. Since the intensity of a given CT transition is a sensitive function of metal−ligand bond covalency, these band assignments imply the presence of strong σ-bonding interactions between the Ni center and the equatorial thiolate and deprotonated amide ligands, in full agreement with our DFT results. As the ligand π-donor set of MOs lack the proper symmetry for significant orbital overlap with the Ni d-based acceptor MOs (i.e., they primarily overlap with the filled Ni(π) orbitals), the S/N(π) → Ni^{3+} CT transitions carry considerably less intensity.

Table 7. Band Assignments for Oxidized and Reduced NiSOD

NiSOD$_{ox}$			**NiSOD$_{red}$**		
band	ν_{max} (cm^{-1})	assignment[a]	band	ν_{max} (cm^{-1})	assignment[a]
1	14 380	Ni(z^2) → Ni(x^2-y^2)	A	17 110	Ni(xz/yz) → Ni(x^2-y^2)
2	15 650	S/N/O(π) → Ni(σ)	B	18 430	
3	18 000		C	20 500	Ni(z^2) → Ni(x^2-y^2)
4	19 920		D	22 240	Ni(xy) → Ni(x^2-y^2)
5	23 290		E	24 970	S(σ/π) → Ni(x^2-y^2)
6	24 700	N/O(σ) → Ni(x^2-y^2)	F	27 650	
7	26 850	S$_6$(σ) → Ni(x^2-y^2)	G	29 220	
8	28 720	S$_2$(σ) → Ni(x^2-y^2)			

[a] The assignments reflect the principal contributors to the electronic excitations. For NiSOD$_{red}$, the LF transitions likely carry some CT character as well.

The Ni(z^2) → Ni($x^2 - y^2$) LF transition is predicted to appear at 14 770 cm^{-1} for the **ox^1** model and at ~16 000 cm^{-1} for the **ox^3** model.[50] These values suggest that this transition gives rise to either band 1 or 2 in the experimental spectra, where the large C_0/D_0 ratio exhibited by band 1 strongly argues in favor of the first option (Table 7). The Ni(π)/Ni(xy) → Ni(σ) LF transitions, which are expected to appear at higher energy, are difficult to assign conclusively. The sizable C_0/D_0 ratios of bands 3 and 5 indicate that the corresponding transitions involve donor MOs possessing significant Ni character, and a general assignment of these bands as S(π)/Ni(π) → Ni(σ) transitions is appropriate, especially given the covalent nature of the NiSOD$_{ox}$ active site. INDO/S-CI calculations for **ox^1** provide further support for this conclusion by predicting a moderately intense Ni(xy) → Ni($x^2 - y^2$) transition at 22 500 cm^{-1}, close in energy to where band 5 is observed in the experimental absorption spectrum.

(b) Reduced NiSOD. Upon Ni^{3+} → Ni^{2+} reduction to generate NiSOD$_{red}$, all CT transitions shift into the UV region, and the weak bands remaining in the visible region arise primarily from LF excitations. The highly covalent nature of the Ni−ligand bonding interactions, though, ensures that these transitions also possess some CT character. According to our DFT and INDO/S-CI calculations, one-electron excitations from the two Ni(π)-based MOs to the unoccupied Ni($x^2 - y^2$)-derived MO yield a pair of transitions that give rise to the lowest-energy absorption feature (bands A and B), while the highest-energy band in the visible region (band D) is due to the Ni(xy) → Ni($x^2 - y^2$) transition. These assignments are fully consistent with the corresponding CD spectrum. In the pseudo-D_{4h} symmetry assumed by the NiSOD$_{red}$ active site, all LF transitions are magnetic-dipole allowed with the exception of the Ni(z^2) → Ni($x^2 - y^2$) transition.[51] Thus, the positive and negative bands

---

(49) The calculated hyperfine splittings arising from equatorial nitrogens are smaller than those from N$_{ax}$ by nearly an order or magnitude.

(50) The INDO/S-CI results for **ox^3** indicate that Ni(z^2) → Ni($x^2 - y^2$) character is distributed over two transitions at 15 390 and 16 820 cm^{-1}. The value reported herein for this model reflects the average of these two energies.

(51) Chang, J. W.; Martin, R. B. *J. Phys. Chem.* **1969**, *73*, 4277−4283.

in the CD spectrum primarily arise from the allowed Ni(π) → Ni($x^2 - y^2$) and Ni(xy) → Ni($x^2 - y^2$) transitions, respectively, and the comparatively weak CD feature (band C) at 20 500 cm^{-1} is then assigned to the Ni(z^2) → Ni($x^2 - y^2$) excitation (Table 7).

Discussion

Recent crystallographic and XAS studies have elucidated the unusual structure of the NiSOD active site in its oxidized and reduced states (Scheme 1).[6,7] NiSOD is the only member of the SOD family to feature thiolate and amide backbone ligation, and the active site exhibits major structural changes upon oxidation/reduction, a feature that it may share with Cu/ZnSODs. Yet, despite these differences, both NiSOD and Fe- and Mn-dependent SODs utilize second-sphere hydrogen-bonding interactions to tune the reactivity of their respective active-site metal ions.[6,7,12] In this study, we have employed numerous spectroscopic and computational tools to elucidate crucial relationships between the geometric and electronic structures of the NiSOD active site. The insights gained from DFT and INDO/S-CI calculations have been combined with the results from our spectroscopic studies to develop experimentally validated bonding descriptions for both the oxidized and reduced states of NiSOD. Comparison of these bonding descriptions to those obtained in parallel computational studies of relevant [NiN_2S_2] complexes illuminate the role of the unique equatorial ligands of NiSOD$_{red}$ in facilitating metal-based oxidation. Additionally, our computational results highlight the importance of second-sphere interactions with respect to the position of the axial imidazole ligand and, in turn, the EPR parameters of NiSOD$_{ox}$. Important conclusions derived from these studies and their implications for the function and mechanism of NiSOD are discussed below.

Although EPR studies have yielded a great deal of information regarding the active-site structure of NiSOD$_{ox}$, this technique is only sensitive to the axial coordination environment, as the unpaired electron resides in a Ni(z^2)-based MO. Conversely, optical spectra of as-isolated NiSOD obtained using absorption, CD, and MCD spectroscopies are dominated by S/N → Ni^{3+} CT transitions, and the corresponding rR spectra exhibit peaks associated with ν(Ni−S) modes. Collectively, these methods are thus extremely well suited to examine the bonding interactions between the Ni center and the equatorial N/S ligands. Our analysis demonstrates that the prominent absorption feature of NiSOD$_{ox}$ at ~27 000 cm^{-1} is composed of three transitions with predominant S/N(σ) → Ni($x^2 - y^2$) CT character (Table 7). The high intensities of these transitions reflect the strongly covalent σ-bonding interactions that exist between the Ni^{3+} center and the equatorial thiolate and deprotonated amide ligands. In comparison, excitations originating from the S/N(π)-based MOs (#87−89) lie lower in energy and are considerably weaker, indicating that these orbitals experience minimal overlap with the Ni(σ)-based acceptor MOs (#90, 91). Based on the large C_0/D_0 ratios exhibited by bands 3 and 5, it appears that many of the transitions involving these ligand π-based MOs derive much of their MCD intensity from mixing with Ni(π) → Ni(σ) LF excitations (Table 1).

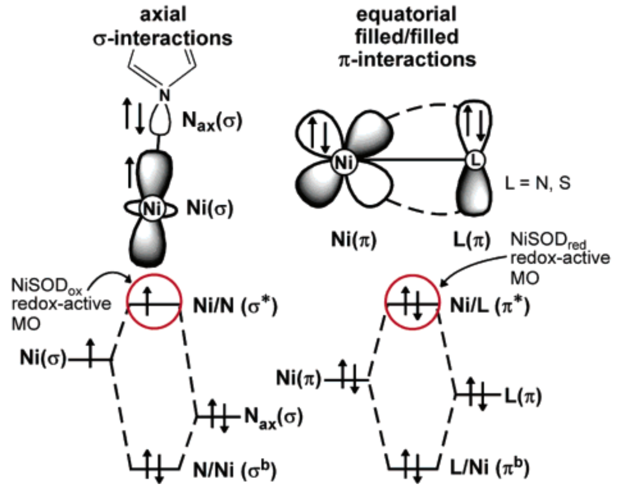

Figure 8. Schematic illustration of the dominant bonding interactions in oxidized and reduced NiSOD. Left: in the NiSOD$_{ox}$ active site, the energy of the sole singly occupied MO is adjusted by a σ-interaction between the Ni(z^2) orbital and the lone pair of the axial N. Right: The HOMO of NiSOD$_{red}$ is destabilized by filled/filled π-interactions between the Ni(π) and L(π) orbitals, where L represents the equatorial thiolate and deprotonated amide ligands.

Despite the low intensities of the S/N(π) → Ni^{3+} CT transitions, our analysis suggests that π-bonding interactions are crucial for NiSOD function. As noted above, the relative orientation of the equatorial ligands ensures that their π-donor orbitals are aligned along the z-axis (Scheme 2), so as to maximize their interactions with the doubly occupied Ni(π) orbitals. This is particularly true in the NiSOD$_{red}$ state, in which the MOs with π-symmetry possess comparable contributions from Ni and ligand orbitals (Table 4). Such bonding interactions between doubly occupied MOs are commonly referred to as "filled/filled interactions" or "four-electron repulsions" and have been frequently used to justify the structures, reactivities, and redox properties of Ni−thiolate complexes,[40,42] as well as a range of other transition metal complexes.[39,52] In the case of NiSOD$_{red}$, these filled/filled interactions between the S/N(π) and Ni(π) orbitals serve to destabilize the two highest-energy occupied MOs, as revealed by our DFT results obtained for the **red** model (Figure 7b), thereby facilitating electron transfer from Ni^{2+} to substrate $O_2^{\bullet -}$ in the catalytic cycle (Figure 8). Moreover, by increasing the Ni orbital character in the redox-active MO of NiSOD$_{red}$, these π-interactions promote Ni^{2+}-based oxidation over S-based oxidation, thereby avoiding the generation of a sulfur radical during step 1b of the catalytic cycle.[53] Our parallel DFT studies of synthetic [NiS_2N_2] complexes suggest that the anionic, π-donating amide ligand of NiSOD is also crucial for encouraging metal-based oxidation and that the presence of a second amide anion (in lieu of the N-terminal amine ligand) would not enhance the Ni d-orbital character in the redox-active MO (Table 5). Thus, the mixed amine/amide ligation of the NiSOD active site ensures Ni^{2+}-based oxidation without depressing the Ni$^{3+/2+}$ redox potential too much for efficient $O_2^{\bullet -}$ oxidation. Note that an additional anionic ligand would also have the detrimental effect of increasing the active site's negative charge, thereby lowering its affinity for the anionic substrate $O_2^{\bullet -}$.

The results obtained in our spectroscopic and computational studies of NiSOD presented above have important implications regarding the nature of the SOD mechanism. The minor spectral

---

(52) (a) Caulton, K. G. *New J. Chem.* **1994**, *18*, 25−41. (b) Ashby, M. T.; Enemark, J. H.; Lichtenberger, D. L. *Inorg. Chem.* **1988**, *27*, 191−197.

perturbations observed in the MCD spectrum when as-isolated NiSOD is treated with azide (Figure 3), a close electronic mimic of superoxide, suggest that small anions cannot coordinate to the Ni^{3+} center but instead bind to nearby residues in the active site. This result supports an outer-sphere mechanism for the $O_2^{\bullet-}$ oxidation step (eq 1a), although the issue of outer-sphere versus inner-sphere mechanisms is certain to remain a matter of dispute. If one assumes an inner-sphere mechanism in the $O_2^{\bullet-}$ reduction step (eq 1b), as proposed in ref 6, the rate constant for electron transfer could be maximized by optimizing overlap between the acceptor orbital of $O_2^{\bullet-}$ and the donor orbital of the Ni^{2+} center. Indeed, the electronic structure of $NiSOD_{red}$ may encourage this type of mechanism, since the π-symmetry of its HOMO would allow for maximal orbital overlap with the singly occupied π^* acceptor orbital of $O_2^{\bullet-}$. Another mechanistic issue concerns the possibility of proton transfer from the thiolate ligands to the substrate. Our experimental and computational results indicate that the strength of the $Ni-S_{Cys}$ bonds in NiSOD is derived from covalent σ-bonding interactions, as the corresponding π-bonding interactions only lead to filled/filled interactions that are effectively nonbonding (Figure 8). Consequently, since protonation at the S atom eliminates these filled/filled repulsions without disturbing the σ-bonding interactions, the Ni−S bonds in our **red-SH** models actually shorten slightly upon thiolate protonation (Table 2), a result consistent with previous synthetic and computational studies of Ni^{2+}−thiolate/thiol complexes.[38] Although the pK_a values for the Cys ligands of NiSOD remain unknown, our computational data suggest that these ligands may indeed function as proton shuttles in the catalytic cycle.

As noted above, previous studies have revealed that square-planar $[Ni^{3+}S_2N_2]^{1-}$ complexes are somewhat unstable in solution,[30,36,54] even though our computational results suggest that the redox-active MO in those species is largely Ni-based. It is therefore tempting to speculate that, to create a fully stable Ni^{3+} species in the enzyme active site, the imidazole group of His1 needs to bind to the metal center following oxidation, thereby forcing the unpaired electron into the $Ni(z^2)$-based MO that possesses little thiolate character (Figure 7a). Indeed, comparison of the experimental $Ni(z^2) \rightarrow Ni(x^2 - y^2)$ transition energies for oxidized and reduced NiSOD suggests that axial coordination of His1 to Ni^{3+} destabilizes the $Ni(z^2)$-based MO by ~6000 cm^{-1} relative to the other Ni-based d orbitals.[55] Structural studies of NiSOD have shown that the axial ligand participates in hydrogen-bonding interactions with conserved second-sphere residues, in particular Glu17, and our DFT computations demonstrate that these interactions influence the ligand's position. By incorporating second-sphere residues into our **ox** models (Figure 5), we were able to lengthen the optimized $Ni-N_{ax}$ bond distance by ~0.10 Å, bringing it closer to the distance found experimentally (Table 2). This axial bond elongation stabilizes the redox-active $Ni(z^2)$-based MO by 0.23 eV (1900 cm^{-1}), which would be expected to shift the redox potential of $NiSOD_{ox}$ by ~200 mV to a more positive value. Thus, similar to the role played by the equatorial N/S ligands in adjusting the reactivity of the reduced state, the axial imidazole ligand functions to tune the redox properties of the oxidized state (Figure 8).

Comparison to $M-S_{Cys}$ Bonding in Other Enzymes. Like NiSOD, blue copper (BC) proteins[44] and superoxide reductases (SORs)[56] function in electron-transfer reactions and contain mononuclear metal centers with mixed N/S_{Cys} ligation. The archetypal BC site found in plastocyanin features a $Cu^{2+/1+}$ center coordinated by Cys, Met, and two His ligands in a distorted tetrahedral geometry. Previous structural and spectroscopic studies have demonstrated that the $Cu-S_{Cys}$ bonding interaction in BC enzymes is very covalent and thus quite strong, resulting in a short bond length of ~2.1 Å.[44] SORs, which catalyze the one-electron reduction of $O_2^{\bullet-}$ to hydrogen peroxide in anaerobic organisms, feature an $Fe^{3+/2+}$ center ligated by four equatorial His residues and an axial Cys ligand in a square-pyramidal geometry. Both BC and SOR proteins have been extensively characterized with structural, spectroscopic, and computational methods, thus providing valuable reference systems with which to compare the metal−thiolate bonding interactions found in other enzymes, such as NiSOD. Below, we compare the spectral and electronic properties of NiSOD characterized herein to those found in similar studies of BC and SOR proteins, with the aim of furthering our understanding of the role of thiolate ligation in promoting catalysis.

The rR spectra reported for oxidized BC[57,58] and SOR[59] proteins exhibit a multitude of peaks in the 250−500 cm^{-1} region that arise from kinematic coupling between the $M-S_{Cys}$ stretching motion and the internal cysteine bending motions. In contrast, the rR spectrum of NiSOD is comparatively sparse, displaying only three intense peaks (Figure 4). The likely origin of this difference lies in the relative orientations of the Cys ligands. Kinematic coupling is maximal for $M-S-C_\beta-C_\alpha$ dihedral angles close to 180° and planar $S-C_\beta-C_\alpha-N$ units,[60,61] and both the BC and SOR proteins satisfy these requirements quite well. On the other hand, examination of the NiSOD crystal structures[6,7] reveals $Ni-S-C_\beta-C_\alpha$ dihedral angles of 45° and 95° for the Cys2 and Cys6 residues, respectively. Furthermore, the $S-C_\beta-C_\alpha-N$ units of Cys2 and Cys6 adopt dihedral angles of 53° and 67°, respectively, suggesting large deviations from planarity. Thus, the orientations of the Cys residues in NiSOD are much less conducive to kinematic coupling. A comparison of the $\nu(M-S_{Cys})$ frequencies is also informative, as these values

---

(53) Under aerobic conditions, two thiolate ligands of nitrile hydratase, a non-heme iron enzyme, are oxygenated to sulfenate and sulfinate donors. Conversely, the thiolate ligands of NiSOD remain unaltered for long periods in air. We have demonstrated herein that the unique ligand environment of Ni^{2+} in $NiSOD_{red}$ ensures that its $1e^-$ oxidation is primarily metal-based. Yet sustained treatment with strong oxidants (like O_2 or H_2O_2) would undoubtedly affect the sulfur ligands, and electronic-structure arguments do not fully account for the lack of reactivity displayed by the thiolates of NiSOD. Instead, the distinct reactivities of the two enzymes presumably reflect intrinsic differences between their active sites; namely, while O_2 can access the thiolate ligands in nitrile hydratase, this may not be the case in NiSOD.

(54) Kruger, H. J.; Holm, R. H. *Inorg. Chem.* **1987**, *26*, 3645−3647.

(55) This estimate is based on the assumption that the relative energy of the $Ni(x^2 - y^2)$-based MO is the same in the oxidized and reduced enzyme. Although not strictly true, this assumption seems reasonable, since the equatorial metal−ligand bonding interactions experience little change upon oxidation/reduction.

(56) Adams, M. W. W.; Jenney, F. E., Jr.; Clay, M. D.; Johnson, M. K. *J. Biol. Inorg. Chem.* **2002**, *7*, 647−652.

(57) (a) Dong, S. L.; Spiro, T. G. *J. Am. Chem. Soc.* **1998**, *120*, 10434−10440. (b) Andrew, C. R.; Sanders-Loehr, J. *Acc. Chem. Res.* **1996**, *29*, 365−372.

(58) Qiu, D.; Dong, S. L.; Ybe, J. A.; Hecht, M. H.; Spiro, T. G. *J. Am. Chem. Soc.* **1995**, *117*, 6443−6446.

(59) Clay, M. D.; Jenney, F. E., Jr.; Noh, H. J.; Hagedoorn, P. L.; Adams, M. W. W.; Johnson, M. K. *Biochemistry* **2002**, *41*, 9833−9841.

(60) (a) Andrew, C. R.; Han, J.; denBlaauwen, T.; vanPouderoyen, G.; Vijgenboom, E.; Canters, G. W.; Loehr, T. M.; Sanders-Loehr, J. *J. Biol. Inorg. Chem.* **1997**, *2*, 98−107. (b) Han, S.; Czernuszewicz, R. S.; Spiro, T. G. *J. Am. Chem. Soc.* **1989**, *111*, 3496−3504.

(61) Han, J.; Adman, E. T.; Beppu, T.; Codd, R.; Freeman, H. C.; Huq, L.; Loehr, T. M.; Sanders-Loehr, J. *Biochemistry* **1991**, *30*, 10904−10913.

correlate with the M$-$S$_{Cys}$ bond strengths. While the high degree of mode mixing in BC proteins complicates determination of the ν(Cu$-$S$_{Cys}$) frequency, ^{32}S $\rightarrow$ ^{34}S isotopic substitution experiments and relative peak intensities provided an estimate of ~420 cm^{-1} for the "uncoupled" ν(Cu$-$S$_{Cys}$) mode in plastocyanin.[58,61] Similarly, the frequency of the ν(Fe$-$S) mode of Fe^{3+}SOR was determined to be ~320 cm^{-1}.[59] The two corresponding modes in NiSOD appear at 349 and 365 cm^{-1}, intermediate between those determined for the oxidized BC and SOR active sites. This trend nicely concurs with the M$-$S$_{Cys}$ bond lengths of ~2.1, 2.2, and 2.35 Å reported for oxidized BC,[62] NiSOD,[6,7] and FeSOR,[63] respectively. Thus, the M$-$S bonds become stronger and more covalent as one progresses from M = Fe^{3+} $\rightarrow$ Ni^{3+} $\rightarrow$ Cu^{2+}. This trend reflects the increased effective nuclear charge of late transition-metal centers, which stabilizes the M d-based MOs relative to the thiolate π-based MOs and thereby increases the covalency of the metal$-$thiolate bonding interactions.

In their oxidized states, BC and SOR each exhibit a prominent absorption band at ~625 nm (16 000 cm^{-1}) that arises from a S$_{Cys}$ $\rightarrow$ M ($\pi \rightarrow \pi^*$) CT transition.[63,64] SOR displays an additional, similarly intense S$_{Cys}$ $\rightarrow$ Fe^{3+} ($\sigma \rightarrow \sigma^*$) CT transition at ~30 000 cm^{-1}.[63] The absorption spectrum of NiSOD$_{ox}$ is notably lacking an intense, low-energy feature; instead, the dominant CT band is now observed in the near-UV region at ~27 000 cm^{-1} (370 nm). This important spectral difference is due to the unique nature of the Ni^{3+}$-$S$_6$/S$_2$ bonds in NiSOD. While the Ni$-$S σ-bonding interactions are strong and covalent, the S(π) orbitals only experience filled/filled interactions with the Ni(π) orbitals, precluding the possibility of S$_{Cys}$ $\rightarrow$ Ni^{3+} ($\pi \rightarrow \pi^*$) CT transitions (Figure 8). As revealed by our DFT computations, these filled/filled π-interactions in NiSOD$_{red}$ assist in redox tuning and facilitate metal-based oxidation. In contrast, the geometry of the BC active site is designed so as to avoid such interactions, thereby promoting delocalization of "hole" character onto the thiolate ligand via Cu$-$S$_{Cys}$ bond covalency. Alternatively, to depress the enzymatic redox potential and facilitate substrate dissociation via a trans influence, the SOR active site promotes covalent σ- *and* π-bonding interactions between Fe^{3+} and the axial thiolate ligand.[56,65] Together, these results provide significant insight into how Nature employs three distinct modes of M$-$S$_{Cys}$ bonding in the BC, SOR, and NiSOD proteins to fine-tune the corresponding active sites for optimum catalytic activity.

Acknowledgment. This research was supported by the NIH (Grant GM 64631 to T.C.B), the University of Wisconsin and the Sloan Foundation Research Fellowship Program (T.C.B.), the NSF Graduate Research Fellowship Program (A.T.F.), the NSF (Grant MCB-0321482 to M.J.M.), the Petroleum Research Fund (M.J.M), and the NIH-Chemistry Biology Interface Program (P.A.B.). We thank Kristina Djinovic Carugo for providing the crystallographic coordinates of NiSOD prior to publication.

Supporting Information Available: Relevant structural parameters and Cartesian coordinates for all DFT geometry-optimized models (Tables S1-4), deconvolutions of absorption and CD spectra of as-isolated NiSOD (Figures S1 and S2, respectively), variable-temperature variable-field MCD data (Figure S3), and computed spectra provided by INDO/S-CI calculations (Figure S4). This material is available free of charge via the Internet at http://pubs.acs.org.

JA042521I

---

(62) Guss, J. M.; Bartunik, H. D.; Freeman, H. C. *Acta Crystallogr.* **1992**, *48*, 790$-$811.

(63) Clay, M. D.; Jenney, F. E., Jr.; Hagedoorn, P. L.; George, G. N.; Adams, M. W. W.; Johnson, M. K. *J. Am. Chem. Soc.* **2002**, *124*, 788$-$805.

(64) Solomon, E. I.; Baldwin, M. J.; Lowery, M. D. *Chem. Rev.* **1992**, *92*, 521$-$542.

(65) (a) Clay, M. D.; Cosper, C. A.; Jenney, F. E., Jr.; Adams, M. W. W.; Johnson, M. K. *Proc. Natl. Acad. Sci. U.S.A.* **2003**, *100*, 3796$-$3801. (b) Fiedler, A. T.; Halfen, H. L.; Halfen, J. A.; Brunold, T. C. *J. Am. Chem. Soc.* **2005**, *127*, 1675$-$1689.